Inorganic Chemistry

pubs.acs.org/IC

Article

Direct ^{17}O Isotopic Labeling of Oxides Using Mechanochemistry

Chia-Hsin Chen, Emeline Gaillard, Frédéric Mentink-Vigier, Kuizhi Chen, Zhehong Gan, Philippe Gaveau, Bertrand Rebière, Romain Berthelot, Pierre Florian, Christian Bonhomme, Mark E. Smith, Thomas-Xavier Métro, Bruno Alonso, and Danielle Laurencin*

Cite This: *Inorg. Chem.* 2020, 59, 13050−13066

Read Online

ACCESS | Metrics & More | Article Recommendations | Supporting Information

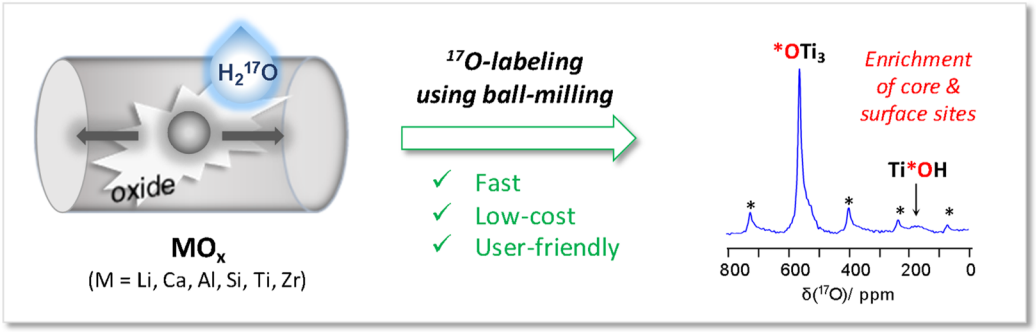

ABSTRACT: While ^{17}O NMR is increasingly being used for elucidating the structure and reactivity of complex molecular and materials systems, much effort is still required for it to become a routine analytical technique. One of the main difficulties for its development comes from the very low natural abundance of ^{17}O (0.04%), which implies that isotopic labeling is generally needed prior to NMR analyses. However, ^{17}O-enrichment protocols are often unattractive in terms of cost, safety, and/or practicality, even for compounds as simple as metal oxides. Here, we demonstrate how mechanochemistry can be used in a highly efficient way for the direct ^{17}O isotopic labeling of a variety of s-, p-, and d-block oxides, which are of major interest for the preparation of functional ceramics and glasses: Li_2O, CaO, Al_2O_3, SiO_2, TiO_2, and ZrO_2. For each oxide, the enrichment step was performed under ambient conditions in less than 1 h and at low cost, which makes these synthetic approaches highly appealing in comparison to the existing literature. Using high-resolution solid-state ^{17}O NMR and dynamic nuclear polarization, atomic-level insight into the enrichment process is achieved, especially for titania and alumina. Indeed, it was possible to demonstrate that enriched oxygen sites are present not only at the surface but also within the oxide particles. Moreover, information on the actual reactions occurring during the milling step could be obtained by ^{17}O NMR, in terms of both their kinetics and the nature of the reactive species. Finally, it was demonstrated how high-resolution ^{17}O NMR can be used for studying the reactivity at the interfaces between different oxide particles during ball-milling, especially in cases when X-ray diffraction techniques are uninformative. More generally, such investigations will be useful not only for producing ^{17}O-enriched precursors efficiently but also for understanding better mechanisms of mechanochemical processes themselves.

INTRODUCTION

Oxygen, as an element, is present in the majority of natural and synthetic materials. It is thus essential to have access to information about the local binding environment around this element to be able to rationalize structure−property relationships in a variety of systems. ^{17}O NMR spectroscopy is one of the most promising spectroscopic techniques for this.[1] Indeed, thanks to the very wide range of variation of the ^{17}O NMR parameters, detailed insight into the bulk and surface structures of a variety of materials can be obtained. For example, recent studies have used ^{17}O NMR to elucidate the structures of porous materials like zeolites and metal−organic frameworks,[2−5] of mixed-metal oxides used as electrode materials,[6,7] or of nanoparticle surfaces.[8−11]

Natural-abundance ^{17}O NMR unfortunately suffers from a very poor absolute signal sensitivity because of the very low abundance of the NMR-active isotope (only 0.04%). This implies that enriching the compounds of interest in ^{17}O is generally necessary to be able to perform high-resolution ^{17}O NMR studies. Until recently, this has actually hampered the large-scale development of ^{17}O NMR spectroscopy because of

Received: January 20, 2020
Published: March 13, 2020

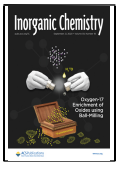

https://dx.doi.org/10.1021/acs.inorgchem.0c00208
Inorg. Chem. 2020, 59, 13050−13066

the lack of cost-efficient and user-friendly enrichment protocols. Indeed, some of the early labeling schemes employed excessive amounts of expensive ^{17}O-enriched precursors ($H_2{}^{17}O$ or $^{17}O_2$) and/or were experimentally constraining because of the need to operate under an inert atmosphere or at high temperatures, or because of excessive experimental times (lasting hours or days).[1,12] In the case of oxides, among the different labeling procedures proposed, those based on sol−gel chemistry have found some success for the preparation of ^{17}O-enriched phases. However, they rely on the availability of metal alkoxide precursors and also require optimization of not only the hydrolysis and condensation steps, but also the drying step in order to remove the alcohol byproduct from the reaction mixture and produce a dry gel that can be then converted into the metal oxide of interest.[12−16] More recently, affordable and practical ^{17}O-enrichment protocols have been proposed[3,17,18] either for direct labeling of the inorganic or hybrid materials of interest or for labeling of the precursors that can then be used for the preparation of these materials. In both cases, mechanochemistry techniques like ball-milling (BM) have been shown to be particularly attractive.[7,18]

In BM, mechanical forces are applied to solid particles, in order to mix them efficiently, alter their size and shape, and make them react at their interfaces.[19,20] The addition of small amounts of liquid during the milling process (typically on the order of 0.1 μL/mg of sample) can have a significant impact on the course of the reactions, such as accelerating their speed.[21] This general approach, which is referred to as "liquid-assisted grinding" (LAG), served as a basis for the development of new ^{17}O-enrichment schemes. Indeed, we showed that using ^{17}O-enriched water as a liquid grinding assistant, it was possible to enrich in ^{17}O a variety of organic and inorganic compounds of synthetic interest, including metal hydroxides like $Mg(OH)_2$, $Ca(OH)_2$, and $Al(OH)_3$.[18] These were then converted into the corresponding metal oxides by heat treatment under an inert atmosphere, leading to the formation of ^{17}O-labeled MgO, CaO and Al_2O_3 (Scheme 1).

Scheme 1. Strategy Previously Proposed for the ^{17}O Labeling of Magnesium, Calcium, and Aluminum Oxides, Starting from Their Hydroxides[18]

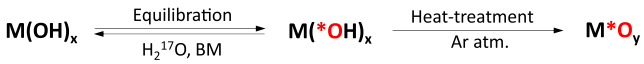

The possibility of easily producing ^{17}O-enriched oxides is highly attractive because these can then be engaged in a variety of reactions using previously established synthetic protocols to prepare enriched ceramics, glasses, or hybrid organic−inorganic materials. However, in order to further broaden the scope of oxides that can be enriched in ^{17}O using mechanochemistry, it appeared to us necessary to look into synthetic approaches that would not require starting from a hydroxide. Indeed, in contrast to $Mg(OH)_2$, $Ca(OH)_2$, and $Al(OH)_3$, a well-defined and stable form of the starting hydroxide may not be readily available, as is the case for titania and silica. Moreover, the initial labeling step of the hydroxide by LAG proceeds by equilibration in the presence of ^{17}O-enriched water (Scheme 1), which is not optimal in terms of the enrichment yield, because the byproduct formed after full isotopic scrambling will be partially enriched H_2*O (with the same ^{17}O-labeling level as the final labeled hydroxide). Using oxides as precursors instead of hydroxides should allow both of these issues to be addressed at the same time. Preliminary evidence that oxides could potentially be directly enriched in ^{17}O using LAG was provided in a recent study in which ^{17}O-labeled alkali transition-metal oxides like Li_2MO_3 (M = Mn, Ru) were synthesized by performing an initial LAG step on nonenriched oxide precursors in the presence of ^{17}O-enriched water, followed by a heat treatment at high temperature.[7] However, no detail regarding the mechanisms by which the isotopic labeling was occurring was proposed, making it difficult to determine at what moment of the reaction the enrichment had taken place and how to adapt this strategy to other materials systems in order to achieve optimal labeling for high-resolution ^{17}O NMR.

In this Article, we study the reactivity of a selection of oxides under LAG using ^{17}O-labeled water, with the overall goal of producing ^{17}O-enriched compounds of synthetic interest for the elaboration of advanced functional materials. First, an improved strategy for preparing Ca*O will be described, with calcium oxide being of interest for the elaboration of bioceramics and bioglasses. Its extension to the synthesis of Li_2*O is also presented, with this precursor being important for preparing electrode materials for lithium-based batteries and ion-conducting glasses. Then, the direct labeling of four widely used oxides of different compositions and crystallinities (silica, alumina, titania, and zirconia) will be discussed, providing insight into the isotopic enrichment process using high-resolution ^{17}O NMR and dynamic nuclear polarization (DNP) analyses. Besides interest for direct and efficient ^{17}O labeling, it will be shown how our approach offers new opportunities for understanding mechanochemical processes at the atomic level.

RESULTS AND DISCUSSION

Improved LAG Approach for the ^{17}O Labeling of s-Block Metal Oxides. We first focused on improving the labeling strategy that we had previously proposed for enriching calcium oxide.[18] More specifically, in order to avoid the initial equilibration step (Scheme 1) and to achieve a better enrichment level of the intermediate hydroxide, we started from the non-labeled oxide CaO and hydrolyzed it by mechanochemistry to produce $Ca(*OH)_2$ (Scheme 2). The idea here is that all of the ^{17}O labels introduced as H_2*O during the LAG step react with CaO to form the ^{17}O-enriched hydroxide.

Scheme 2. Alternative Strategy Proposed Here for the ^{17}O Labeling of CaO

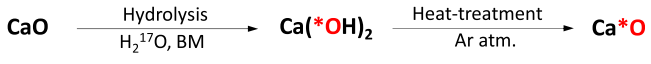

The BM conditions required to perform the hydrolysis step were initially tested using non-labeled water, by analyzing the reaction medium by powder X-ray diffraction (PXRD). It was found that, after 1 h of milling of CaO at 25 Hz in the presence of 1 equiv of water, complete conversion into the hydroxide phase occurred. Using these synthetic conditions with ^{17}O-enriched water, ^{17}O-labeled $Ca(*OH)_2$ was then obtained, as shown by PXRD (Figure 1a) and solid-state ^{17}O magic-angle-spinning (MAS) NMR (Figure 1b, top). This phase could then be transformed into enriched Ca*O by heat treatment under an inert atmosphere (Figure 1b, bottom).

https://dx.doi.org/10.1021/acs.inorgchem.0c00208
Inorg. Chem. 2020, 59, 13050−13066

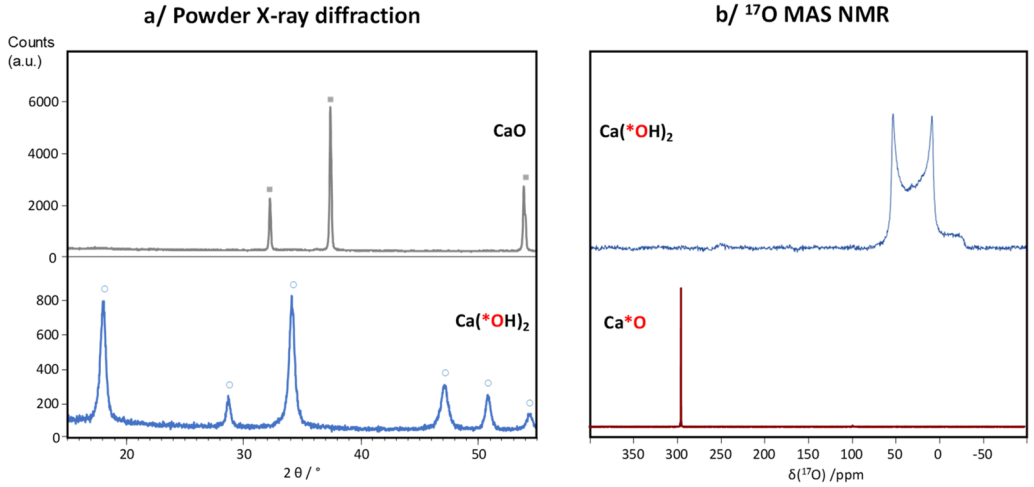

Figure 1. (a) PXRD analyses before and after LAG: CaO precursor obtained after the heat treatment of commercial $Ca(OH)_2$ (top) and enriched phase recovered after LAG in the presence of H_2*O (bottom). The symbols ■ and ○ correspond to the diffraction peaks expected for CaO (ICSD 163628) and $Ca(OH)_2$ (ICSD 15471), respectively. (b) Solid-state ^{17}O NMR spectra of ^{17}O-enriched $Ca(*OH)_2$ (prepared by LAG of CaO using $H_2{}^{17}O$) and Ca*O (obtained after the heat treatment of $Ca(*OH)_2$). These ^{17}O MAS NMR spectra are in agreement with previous measurements at this magnetic field.[18]

On the basis of the above, it is clear that direct conversion of oxides like CaO into their hydroxides can be achieved by BM in the presence of stoichiometric amounts of ^{17}O-enriched water, which is an improvement for the production of labeled hydroxides like $Ca(*OH)_2$.[18] Using a similar approach, the labeling of other s-block oxides like Li_2O could be achieved, which provide attractive alternatives in comparison to the existing protocols,[22,23] as discussed in Supporting Information S1. As detailed below, extension of this type of approach to oxides of the p and d blocks was then studied, in order to expand the scope of precursors that could be enriched by this technique.

^{17}O Labeling of p and d-Block Oxides Using LAG. *Enrichment of SiO_2, Al_2O_3, TiO_2, and ZrO_2: Structural Analyses after 1 h of LAG.* Silica, alumina, titania, and zirconia were selected for ^{17}O-labeling tests on p- and d-block oxides because of their numerous uses for the preparation of functional materials. For each of these phases, the starting materials were commercially available porous samples with relatively high surface areas (all above 80 m^2/g) because this was expected to favor surface reactions with the enriched water during BM. On the basis of scanning electron microscopy (SEM) and PXRD analyses, each precursor was initially composed of agglomerated nanoparticles of ∼10−20 nm diameter but with different crystallinities. Indeed, while the silica precursor was fully amorphous, the three others gave diffraction peaks in X-ray diffraction (XRD), which could be assigned to the anatase phase for titania, to the monoclinic polymorph for zirconia, and to a mixture of γ and δ polymorphs for alumina (Figure 2, insets).

Each compound was milled in the presence of stoichiometric amounts of ^{17}O-enriched water, for durations of up to 1 h. The initial LAG conditions were set such that 1 equiv of "MO_y" (y = 2 for M = Si, Ti, and Zr and $y = {}^3/_2$ for M = Al) was reacted with $y/2$ equiv of H_2*O as a means to minimize losses of H_2*O if the BM hydrolysis reaction were to be incomplete. Milled samples were characterized by PXRD, N_2 adsorption/desorption isotherms, SEM, energy-dispersive X-ray spectroscopy (EDXS), and ^{17}O MAS NMR (Figure 2 and S2−S5).

After 1 h of LAG, no new phase was observed by PXRD, and the diffractograms of all phases were essentially the same as those recorded before milling (Figure 2, insets). In SEM, the presence of agglomerated nanoparticles could still be observed, without any significant change in the particle size, except in the case of silica, for which nanoparticles appeared to have merged into larger entities. More striking differences were found in the N_2 adsorption/desorption isotherms of all oxides before and after milling (Figures S2−S5) because of changes in the surface area and/or pore geometry. In the case of silica, a decrease in the porosity was observed (with the surface area being reduced by a factor of ∼3), while in the case of alumina, the main change concerned the pore geometry (because the surface area remained essentially the same as that before milling). For titania and zirconia, the differences in the isotherms revealed that both a reduction in the surface area and a change in the pore geometry had occurred, pointing to significant surface reconstruction taking place during milling. In order to understand the changes in texture of the different oxides, high-resolution NMR experiments were performed.

All four materials were analyzed by solid-state ^{17}O NMR (Figure 2). The spectra obtained show that in all cases the labeling was successful. Indeed, for each oxide, ^{17}O NMR resonances attesting to the formation of a significant proportion of *OM_x environments (M = Si, Al, Ti, Zr) were observed. In the case of silica, the observed quadrupolar line shape is consistent with enriched siloxanes (Si−*O−Si), as shown by the fit of the ^{17}O MAS NMR spectrum (Figure S7).[1,24,25] Concerning alumina, two broad resonances are observed, with the high-frequency contribution (centered at ∼60 ppm at 14.1 T) coming from various *OAl_x environments (x = 3, 4)[12,25,26] and the other originating from *OH groups, as further discussed below. In the case of titania, the main ^{17}O resonance is centered at ∼560 ppm, which corresponds to the *OTi_3 environments of anatase.[27,28] Regarding zirconia, two sharp resonances are observed, which are centered at 325 and 403 ppm, and correspond to the *OZr_4 and *OZr_3 environments of the monoclinic form.[14,27,29] For the latter two phases, it is particularly noteworthy that the main ^{17}O NMR resonances detected are those of crystalline environ-

https://dx.doi.org/10.1021/acs.inorgchem.0c00208
Inorg. Chem. 2020, 59, 13050−13066

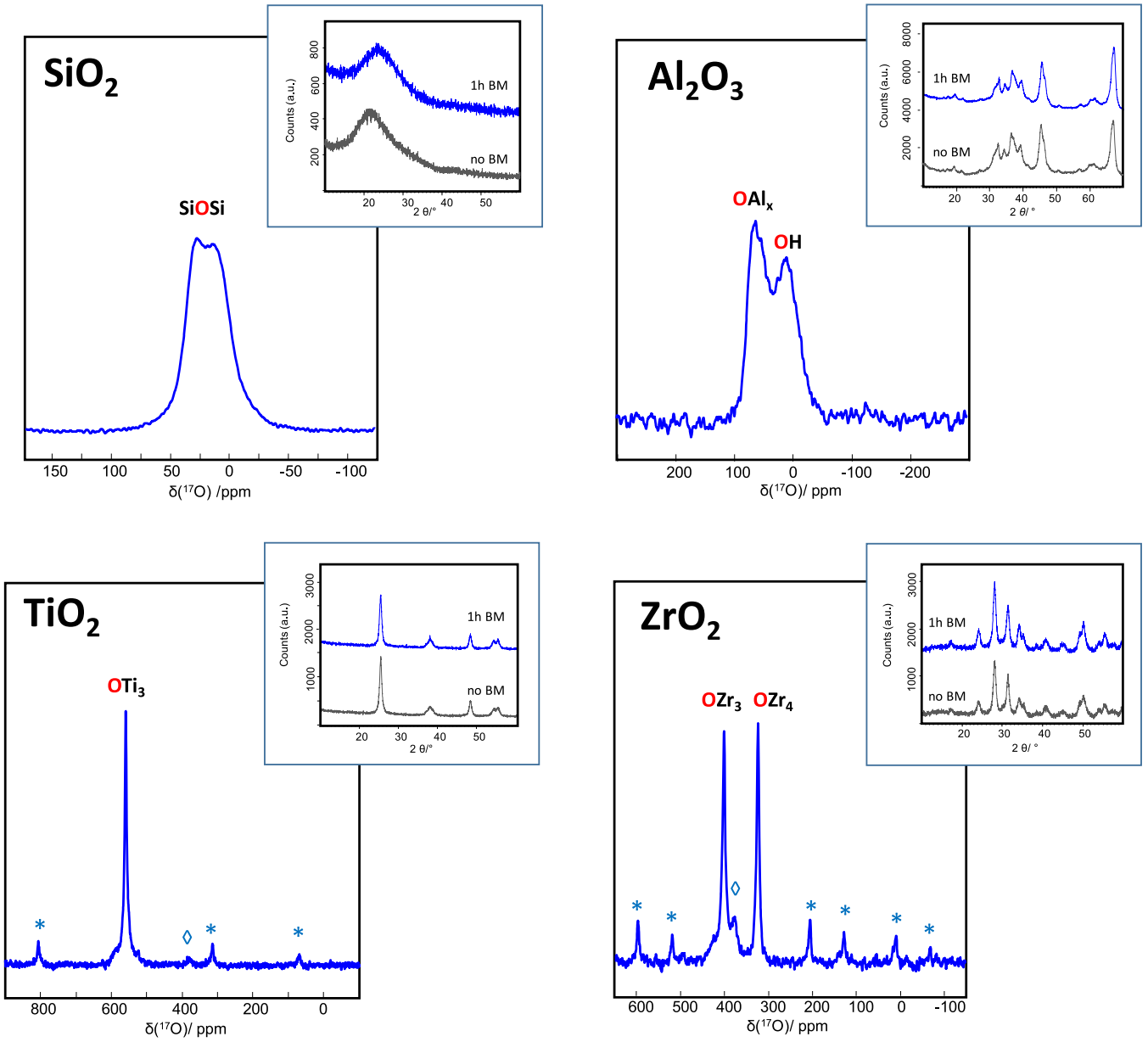

Figure 2. ^{17}O MAS NMR spectra recorded at 14.1 T for the SiO_2, Al_2O_3, TiO_2, and ZrO_2 phases after 1 h of BM in the presence of $H_2{}^{17}O$ (followed by drying under vacuum at room temperature). The insets show the PXRD patterns before (gray) and after (blue) 1 h of BM in the presence of $H_2{}^{17}O$. The symbols * correspond to spinning sidebands and the symbols ◇ to the zirconia rotor background signal (Figure S6a). All NMR acquisition conditions are provided in Table S1.

ments of titania (anatase form) and zirconia (monoclinic form). Hence, although XRD had not revealed any strong changes during the LAG step, ^{17}O NMR shows that a significant restructuring of the four oxides actually occurs, which leads to the breaking/formation of multiple M−O bonds and eventually results in a significant proportion of enriched $*OM_x$ core-like environments.

The solid-state ^{17}O NMR data also reveal that the overall ^{17}O-enrichment level is high (see Figure S6b for a comparison with natural-abundance data). More quantitative analyses were carried out on the silica and titania samples using surface-ion mass spectrometry (SIMS) in order to determine the absolute enrichment after the LAG step. Measurements were performed on ^{18}O-enriched samples, which were prepared using a procedure similar to that above but with 97% ^{18}O-labeled water to achieve better quantification by SIMS. Under these conditions, given that 1 equiv of H_2*O is reacted with 1 equiv of MO_2 (M = Si, Ti), the maximum enrichment was expected to be ∼32% (i.e., ∼97/3) in the case of complete isotopic scrambling of the oxygen sites during the $H_2{}^{18}O$ LAG. After 1 h of LAG (followed by drying at room temperature under vacuum), the ^{18}O enrichments determined by SIMS were 27% for silica and 15% for titania. This demonstrates that the isotopic scrambling was indeed nearly complete for silica under the milling conditions used here but that a higher enrichment level is potentially achievable for titania. From a more general perspective, considering that the natural abundance of ^{17}O is only 0.04%, these analyses confirm that high enrichment levels of oxides can be easily reached by LAG in just 1 h, using stoichiometric amounts of enriched H_2*O.

Insight into the Labeling Mechanisms: NMR Analyses after Different LAG Times. Given that the source of ^{17}O is

https://dx.doi.org/10.1021/acs.inorgchem.0c00208
Inorg. Chem. 2020, 59, 13050−13066

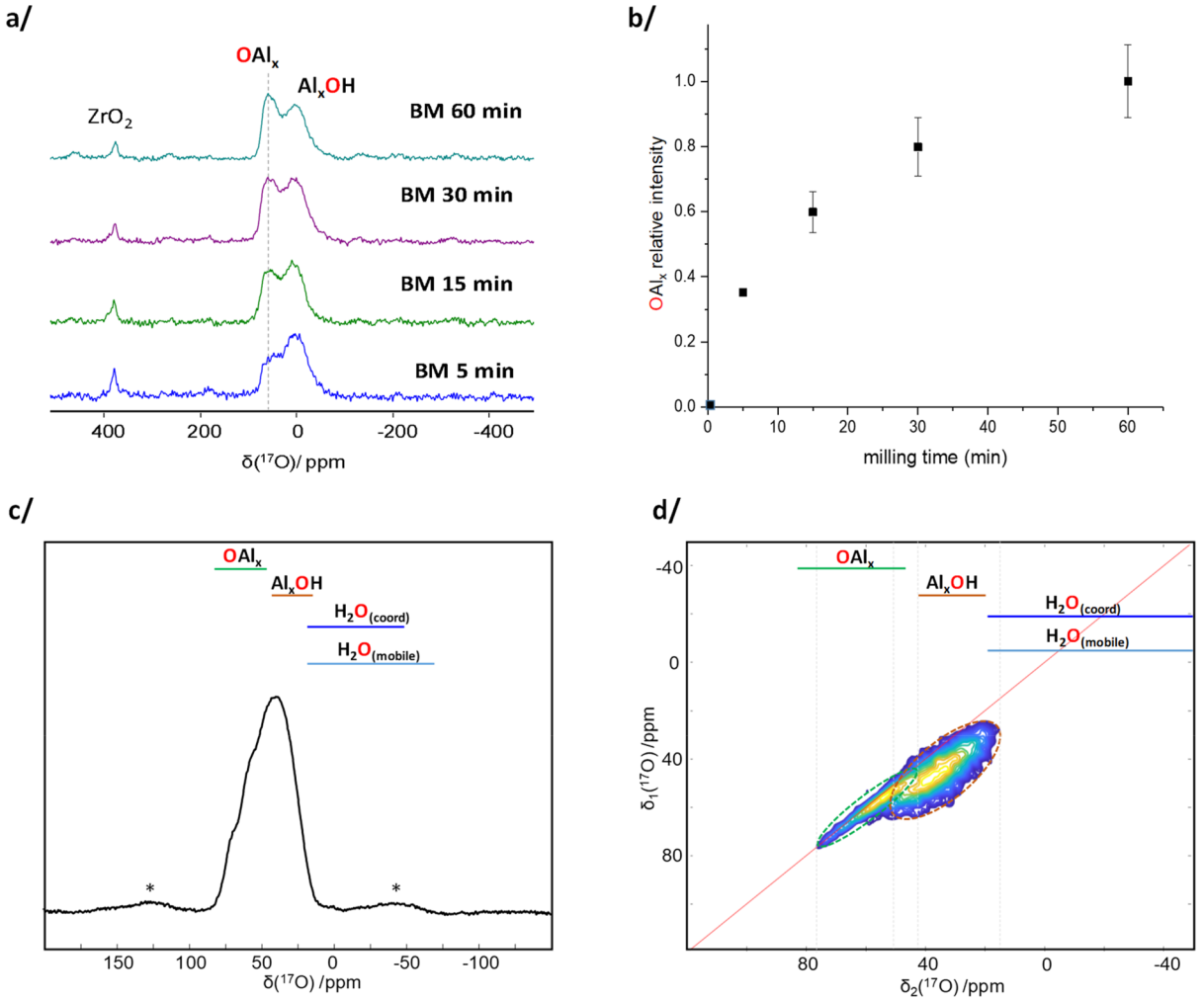

Figure 3. (a) Quantitative single-pulse ^{17}O MAS NMR spectra, recorded at 14.1 T for Al_2O_3 phases obtained after different milling times in the presence of $H_2{}^{17}O$, followed by drying under vacuum at room temperature (all spectra were acquired over 18 h, using a $\pi/12$ excitation pulse and a recycle delay of 16 s). (b) Evolution of the relative proportion of *OAl$_x$ sites as a function of the milling time, as determined by quantifying the relative intensity of the *OAl$_x$ signal to that of the natural-abundance zirconia rotor peak (spectra shown in part a/ of this figure) and normalizing the mass of the sample introduced in the rotor (Figure S9). (c) ^{17}O MAS NMR spectrum recorded at 35.2 T for an Al_2O_3 phase enriched in ^{17}O by LAG after 15 min of grinding, followed by drying the sample at room temperature (this spectrum was recorded using a much shorter recycle delay and different excitation scheme than those in Figure 3a). (d) ^{17}O MQMAS NMR spectrum recorded at 35.2 T, in which the *OAl$_x$ (dashed green circle) and Al$_x$-*OH (dashed brown circle) sites are resolved. The colored bars above the spectra in parts c and d correspond to the shift ranges expected for different oxygen environments, based on the literature.[12,25,26,31,32] Acquisition conditions can be found in Table S1. The symbols * correspond to spinning sidebands.

enriched water, it is reasonable to propose that part of the labeled *OM$_x$ sites have formed by condensation reactions involving intermediate M−*OH species (M = Si, Al, Ti, Zr). Additional multinuclear NMR analyses at different milling times were thus performed on each of the oxides to gain more insight into the enrichment mechanisms. The most complete studies were carried out on alumina and titania, as described below.

Alumina. Quantitative ^{17}O NMR analyses were performed on alumina phases recovered after different LAG times (between 5 min and 1 h). In all cases, two main resonances were observed at 14.1 T, which were centered at ∼9 and 60 ppm. As mentioned above, the higher-frequency signal corresponds to *OAl$_x$ environments, and its intensity was found to gradually increase with the milling time (Figure 3a,b). This is all the more interesting that no significant changes could be observed for these samples in the XRD patterns or in the ^{27}Al MAS and ^{27}Al{^{1}H} cross-polarization MAS (CPMAS) NMR spectra (aside from the appearance of a very weak Al^{V} signal after 1 h of BM, as shown in Figure S8). These observations confirm that ^{17}O NMR can provide unique insight into both structural and kinetic aspects of the bonding rearrangements occurring at the atomic level during BM for this system.

The broad low-frequency signal (centered at ∼9 ppm) is consistent with labeled *OH groups. Given that both Al$_x$OH species and water molecules can potentially be found in this chemical shift range at 14.1 T,[25,26,30−32] additional characterizations were performed at ultrahigh magnetic field (35.2 T) to reduce the effect of second-order quadrupolar broadening[12] and discriminate better the *OH and H_2*O species. In a comparison of the 1D MAS spectrum at 35.2 T to the data reported in the literature,[4,25,31,32] it appears that few ^{17}O-enriched water molecules are likely to be present, meaning that the majority of enriched *OH groups correspond to Al$_x$-*OH species (Figure 3c). In order to achieve higher resolution,

https://dx.doi.org/10.1021/acs.inorgchem.0c00208
Inorg. Chem. 2020, 59, 13050−13066

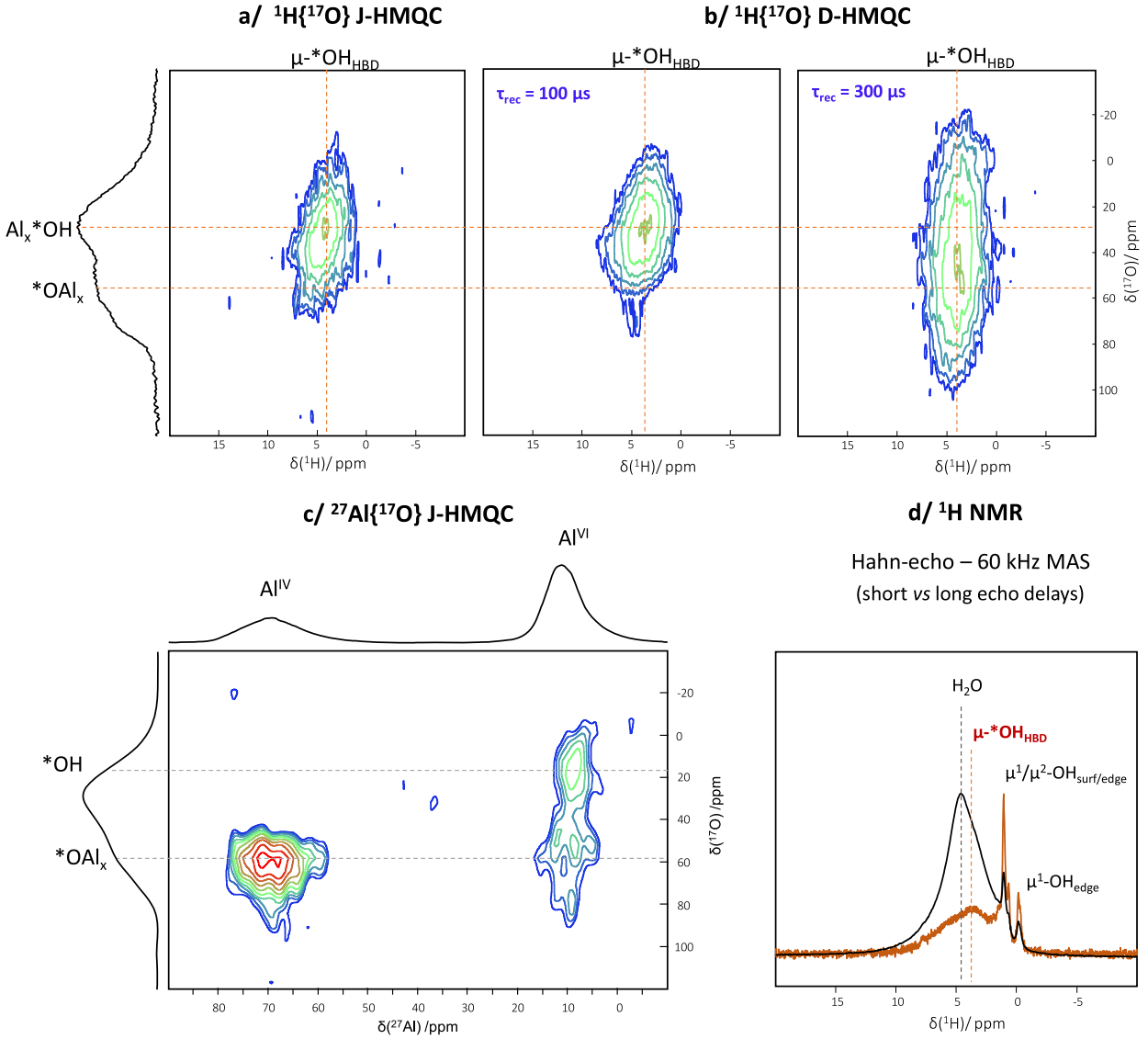

Figure 4. (a) ^{1}H{^{17}O} J-HMQC NMR spectrum recorded at 20.0 T and 60 kHz MAS on an Al_2O_3 phase enriched in ^{17}O by LAG after 15 min of grinding, followed by drying the sample at room temperature. The projection corresponds to the double-frequency sweep (DFS)-1 pulse signal for this phase. (b) ^{1}H{^{17}O} D-HMQC NMR spectra recorded at 20.0 T and 60 kHz MAS on the same phase, using two different recoupling times (100 and 300 μs). (c) ^{27}Al{^{17}O} J-HMQC NMR spectrum recorded at 20.0 T for an Al_2O_3 phase enriched in ^{17}O by LAG (15 min of BM), after drying under vacuum at room temperature (the total acquisition time was ~50 h for this spectrum). Projections correspond to Hahn echo spectra recorded for the sample at this magnetic field. (d) ^{1}H Hahn echo NMR spectra recorded at 20.0 T and 60 kHz MAS, using echo delays of 2 (black) and 50 (brown) rotor periods (see Figure S10 for a comparison to the background ^{1}H NMR spectrum). ^{1}H resonances are assigned based on recent literature (HBD = hydrogen-bond donor).[34]

complementary analyses were performed using the ^{17}O multiple quantum MAS (MQMAS) sequence.[33] This allowed the Al$_x$-*OH sites to be more clearly separated from the *OAl$_x$ ones (Figure 3d, dashed circles). Moreover, it revealed a significant distribution in the ^{17}O chemical shifts for both types of sites, each of which spans more than 30 ppm. This means that there are several different *local* environments for the enriched oxygen sites, possibly because of variations in the hydrogen-bonding network around them and/or in the number and type of Al^{3+} cations to which they are bound. To analyze this in more detail, additional high-resolution ^{1}H−^{17}O and ^{27}Al−^{17}O heteronuclear correlation experiments were carried out.

The different types of protons present around the enriched oxygen sites were studied using fast ^{1}H{^{17}O} MAS HMQC (heteronuclear multiple quantum coherence) NMR experiments at high magnetic field (20.0 T), looking at through-bond connectivities (J-HMQC) as well as through-space proximities (D-HMQC). The main crosspeak observed on the 2D J-HMQC spectrum correlates the low-frequency ^{17}O resonance (Al$_x$-*OH) to a ^{1}H resonance centered at ~3.8 ppm (Figure 4a). This ^{1}H chemical shift is consistent with a surface OH group acting as a hydrogen-bond donor (denoted here as μ-OH$_{HBD}$).[34] The significant line width of the ^{1}H resonance points to a distribution in the μ-OH$_{HBD}$···O bond distances and angles.[34,35] Complementary 2D D-HMQC experiments were carried out to further characterize these hydroxyl environments (Figure 4b). At a short recoupling time (τ_{rec} = 100 μs), the D-HMQC spectrum provides conclusions similar to those of the J-HMQC experiment, given that only

https://dx.doi.org/10.1021/acs.inorgchem.0c00208
Inorg. Chem. 2020, 59, 13050−13066

correlations to the closest hydrogen atoms appear in these conditions, i.e., with hydrogen atoms that are directly bound to ^{17}O. In contrast, at longer recoupling times (τ_{rec} = 300 μs), an additional correlation is observed with *OAl$_x$ resonances. This points to the close proximity of some of the μ-OH$_{HBD}$ protons to *OAl$_x$ sites, possibly due to μ-OH$_{HBD}$···*OAl$_x$ hydrogen bonds. It is worth noting that recent computational studies of γ-alumina surfaces suggest that μ-OH$_{HBD}$···OAl$_x$ hydrogen bonds can indeed be present at the surface.[34] The diversity of hydrogen-bonding environments of surface hydroxyls can thus account, at least in part, for the distribution in oxygen environments around the Al$_x$-*OH and *OAl$_x$ moieties mentioned above (Figure 3d).

To go one step further, a ^{27}Al{^{17}O} J-HMQC experiment was performed to see which of the hexacoordinate (Al^{VI}) and tetracoordinate (Al^{IV}) sites of alumina were linked to *OAl$_x$ and Al$_x$-*OH moieties (Figure 4c). Three crosspeaks are observed on the 2D spectrum, which provide direct evidence of the presence of Al^{VI}-*OH, Al^{VI}-*O, and Al^{IV}-*O bonds. Considering the *OAl$_x$ sites, this spectrum clearly shows that part of the chemical shift distribution observed in Figure 3d can come not only from the number but also from the type of aluminum atoms attached to the oxygen sites (Al^{IV} and/or Al^{VI}).

The lack of Al^{IV}-*OH correlations in Figure 4c may seem surprising when considering the ^{1}H MAS NMR data (see Figures 4d and S10). Indeed, the 1D ^{1}H NMR spectrum (which was recorded using two different echo delays to achieve better resolution) shows sharp resonances, notably at ∼− 0.2, 0.7, and 1.1 ppm. On the basis of the literature, these could correspond to terminal (μ^1-OH) and bridging (μ^2-OH) sites,[34,36] located at the surfaces and edges of alumina particles. In particular, the signal at −0.2 ppm has recently been attributed to μ^1-OH species present at the edges,[34] which are likely to be linked to tetrahedral Al^{IV} sites.[36] This would imply that while Al^{IV}OH species appear to be present in the sample, they could not be detected in ^{17}O NMR. Several explanations can be proposed for this. First, this observation could be consistent with the known difference in reactivity of the different surface hydroxyls.[34,37] Indeed, it is possible that, upon exposure of the sample to air and hence ambient humidity (when recovering the sample after the LAG step or during the packing/unpacking of NMR rotors), some of the enriched Al-*OH groups back-exchange with non-labeled hydroxyls. The fact that the samples are still porous after LAG would indeed be in favor of surface exchanges of reactive OH groups, which would be more likely to occur for the hydroxyls that are more reactive and/or less tightly bound, as would be the case for μ^1-OH and μ^2-OH groups with ^{1}H resonances below 3 ppm, which are not involved in strong hydrogen bonds.[34] This exchange would also be consistent with the fact that, on the ^{1}H{^{17}O} J-HMQC data, only the ^{1}H resonances of the hydrogen-bonded μ-OH groups at ∼3.8 ppm correlate to the Al$_x$-*OH resonance but not those at ∼−0.2, 0.7, and 1.1 ppm (due to their back-exchange). Second, from a purely NMR perspective, it is also possible that the small proportion of μ^1-OH and μ^2-OH resonances (shown by ^{1}H NMR), combined with potentially smaller values of J couplings, renders them "invisible" in the 2D ^{27}Al{^{17}O} NMR experiment (Figure 4c). All of the above reasons could explain (at least in part) why no cross-peak correlating Al^{IV} sites to OH groups could be observed on the ^{27}Al{^{17}O} J-HMQC NMR spectrum.

The observation of the progressive formation of *OAl$_x$ sites (Figure 3b), and the potential back-exchange of some of the enriched hydroxyls, prompted us to use ^{17}O DNP−surface-enhanced NMR spectroscopy (SENS)[38,39] to examine the nature of the oxygen environments present at the *surface* of the alumina particles. DNP analyses were performed on a sample recovered after 15 min of milling, after impregnation by a biradical solution of TEKPol in deuterated tetrachloroethane. Two types of NMR sequences were used as a means to polarize differently the surface oxygen atoms during microwave irradiation: (i) direct-excitation ^{17}O NMR (preceded by a DFS enhancement) in order to polarize the surface oxygen sites directly from the radical and (ii) ^{17}O{^{1}H} CPMAS NMR, where ^{17}O sites are detected based on their relative proximity to the protons polarized by the biradical (by varying the contact time used). In both situations, the ^{17}O NMR signals of *OAl$_x$ and *OH groups were found to be enhanced upon microwave irradiation (Figure 5), suggesting that both of these ^{17}O environments are present at the surface of the alumina particles. In particular, under ^{17}O{^{1}H} DNP CPMAS NMR conditions (Figure 5), both sites were enhanced by a factor of ∼4, meaning that protons located at the surface of the particles after LAG can transfer their polarization to neighboring Al-*OH (at short contact time) and *OAl$_x$ (at longer contact time) sites. Although these DNP−SENS experiments did not allow any absolute quantification of the relative labeling of the bulk or surface of the material, they clearly suggest that some

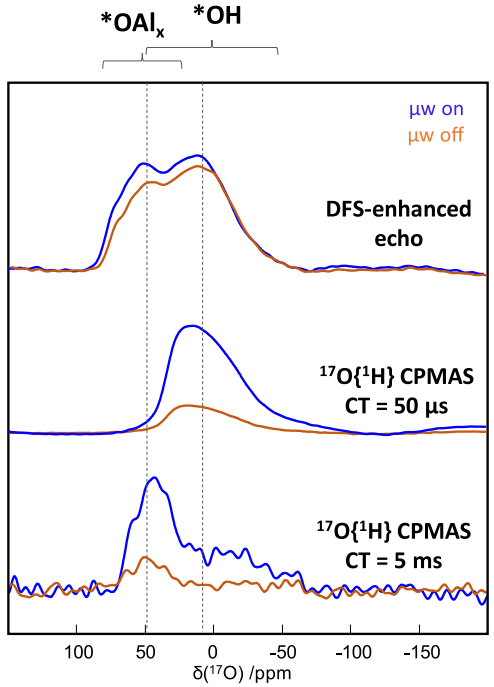

Figure 5. ^{17}O DNP experiments carried out at 14.1 T on an Al_2O_3 phase enriched in ^{17}O by 15 min of LAG (followed by drying the sample at room temperature) and impregnation by TEKPol/D_2-TCE: (i) direct-excitation ^{17}O DNP NMR spectra (with a DFS enhancement) and (ii) ^{1}H{^{17}O} CPMAS DNP NMR spectra recorded at 50 μs and 5 ms contact times (CT). Spectra recorded without (brown) and with (blue) microwave irradiation are compared (μw on/μw off). DNP acquisition conditions and enhancements are discussed in Supporting Information S11 and comparisons to ^{17}O NMR data recorded at room temperature are reported in Figure S12.

https://dx.doi.org/10.1021/acs.inorgchem.0c00208
Inorg. Chem. 2020, 59, 13050−13066

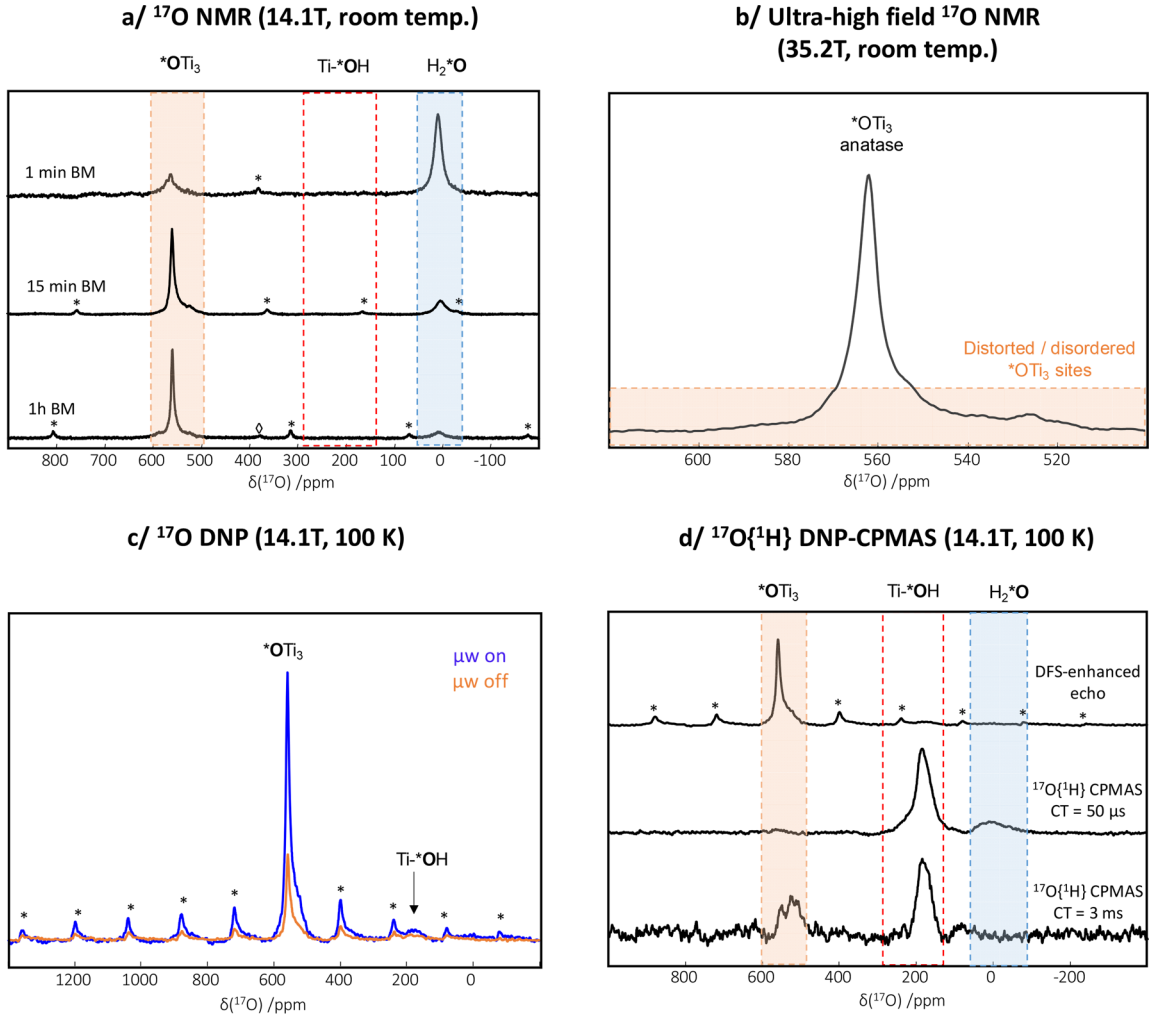

Figure 6. (a) ^{17}O MAS NMR spectra recorded at 14.1 T on "fresh" TiO_2 phases enriched in ^{17}O by LAG (for 1 min, 15 min, and 1 h milling times). (b) ^{17}O MAS NMR spectrum recorded at 35.2 T on a TiO_2 phase enriched in ^{17}O by LAG (15 min of BM), after drying under vacuum at room temperature. (c) ^{17}O DNP NMR spectrum of a TiO_2 phase enriched in ^{17}O by LAG (15 min of BM), after drying under vacuum at room temperature, and impregnation by a 16 mM solution of TEKPol in tetrabromoethane (spectra recorded at ∼100 K with and without microwave irradiation). (d) $^{17}O\{^1H\}$ DNP CPMAS NMR spectra recorded at 50 μs and 3 ms contact times, in comparison to the DFS-enhanced echo spectrum recorded at ∼100 K. All acquisition parameters can be found in Table S1. The symbols * correspond to spinning sidebands, and the symbol ◇ corresponds to the zirconia rotor background signal.

enriched oxygen sites are still present at the surface of the particles, despite possible partial $^{17}O/^{16}O$ back-exchanges upon exposure of the sample to an ambient atmosphere.

In summary, although the overall structure of alumina appears to be maintained during the LAG step (according to XRD and ^{27}Al NMR), part of this phase actually undergoes several reactions in the presence of H_2O, leading to a change in the texture of the material and to the formation of Al_x-*OH and *OAl_x species. The fact that *OAl_x environments were detected after only 5 min of milling underscores that the condensation of Al_x-*OH groups proceeds very quickly under the reaction conditions used here. For both Al_x-*OH and *OAl_x species, high-resolution NMR experiments were able to shed light on the diversity of oxygen local environments because of the presence of hydrogen bonds and differences in the nature and number of aluminum sites to which they are bound. Moreover, ^{17}O DNP−SENS experiments were performed, suggesting that some of the enriched Al_x-*OH and *OAl_x sites are located at the surface of the particles.

Titania. Enriched titania phases were studied by ^{17}O MAS NMR after different LAG times (1 min, 15 min, and 1 h). NMR spectra were recorded both on "fresh" samples, which were analyzed by NMR directly after milling, and on samples that had undergone an additional drying step at room temperature. In all cases, signals belonging to *OTi_3 environments were observed around 550 ppm. The resonance characteristic of crystalline anatase was found to increase with the milling time (signal at 560 ppm in Figure 6a). Weaker underlying resonances, which span between 500 and 600 ppm (Figure 6b), were also observed at all milling times and can be ascribed to more distorted/disordered *OTi_3 environments and surface defects.[9,28,40]

In the case of the "fresh" phases, residual ^{17}O labeled water was detected at ∼0 ppm. Its relative proportion was found to decrease as the milling time increased (Figure 6a). However, no clear evidence of Ti-*OH groups was observed. On the basis of the literature, Ti-*OH resonances were expected to be centered just above 200 ppm.[9,40,41] Complementary ^{17}O DNP−SENS analyses were thus carried out to try to detect

https://dx.doi.org/10.1021/acs.inorgchem.0c00208
Inorg. Chem. 2020, 59, 13050−13066

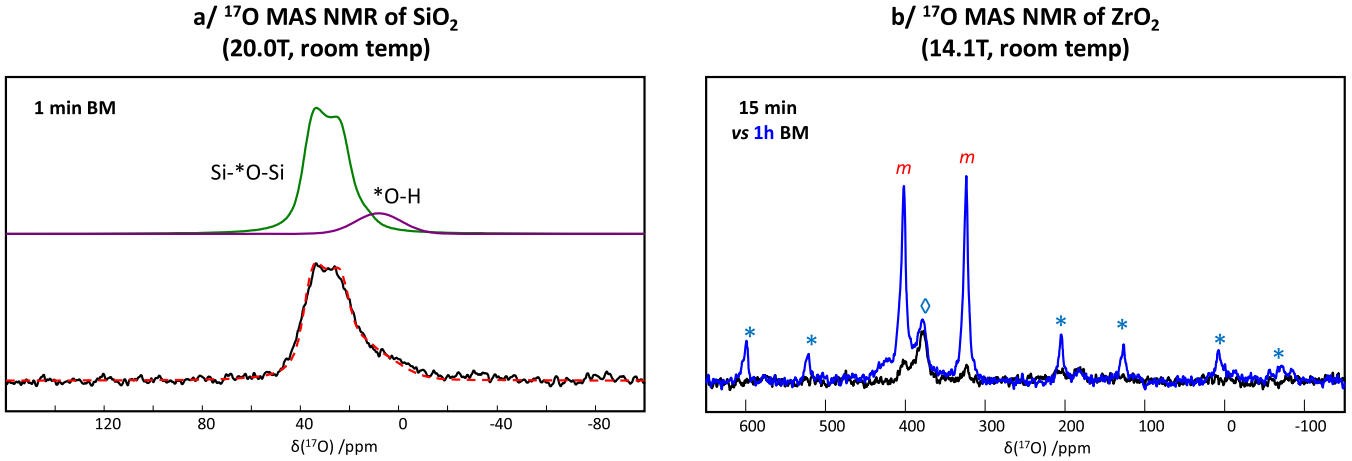

Figure 7. (a) ^{17}O MAS NMR analysis performed at 20.0 T and 60 kHz MAS on a SiO_2 phase enriched in ^{17}O by LAG (1 min BM), after drying under vacuum at room temperature. The fit (dashed red line) was performed considering siloxanes (green) and silanols (purple). The silanol resonances could be more clearly resolved using ^{17}O{^{1}H} CPMAS NMR analyses at short contact times (Figure S13), and their NMR signature is consistent with previous reports.[24,45] (b) ^{17}O MAS NMR analyses performed at 14.1 T and 20 kHz MAS on a ZrO_2 phase enriched in ^{17}O by LAG, after 15 min (black) and 1 h (blue) of milling. The "m" symbols indicate the two main resonances of monoclinic zirconia. The symbols * correspond to spinning sidebands, and the symbol ◇ corresponds to the zirconia rotor background signal (Figure S6).

more clearly the surface species (Figure 6c,d) and bring direct evidence of Ti*OH groups (if any). First, it is worth noting that at low temperatures, such as those used for DNP analyses (~100 K), a very weak signal could be detected at ~200 ppm, suggesting the presence of a small number of Ti-*OH species. Dynamics within the Ti-*OH moieties at room temperature may explain why they could not be detected by conventional NMR. This signal could then be enhanced by direct-excitation ^{17}O DNP (Figure 6c) and even more so using ^{17}O{^{1}H} DNP CPMAS experiments at very short contact times (Figure 6d). Indeed, the main signal observed by ^{17}O{^{1}H} DNP CPMAS for 50 μs contact time was centered at ~200 ppm.

On the basis of previous experimental and computational studies reported in the literature, the extent of water dissociation on anatase surfaces is known to be highly dependent on several parameters, including the nature of the surface exposed and the extent of surface defects.[42,43] Hence, it is possible that the formation of Ti-*OH groups by dissociation of H_2*O on anatase requires the creation of reactive surfaces by mechanochemistry. Moreover, given that very few Ti-*OH species could be detected at the surface of the materials (even for "fresh" phases), it is possible that these recondense quickly to form *OTi$_x$ sites under the reaction conditions used here. Overall, this would explain the evolution of the reaction medium shown in Figure 6a.

DNP−SENS analyses were able to provide additional information regarding the other enriched oxygen sites, which were present close to the surface, aside from the Ti-*OH moieties. First, upon analysis of the results of the DNP experiments performed with direct ^{17}O acquisition (Figure 6c), it is clear that bulklike *OTi$_3$ environments are also present close to the surface of the particles. Second, by increasing the contact time in the ^{17}O{^{1}H} DNP CPMAS experiment, it was possible to observe weak resonances in the *OTi$_3$ region (Figure 6d, CT = 3 ms). These correspond to oxygen species that are spatially close to protons (but not directly bound to them) and appear to contribute to the "underlying" disordered/distorted *OTi$_3$ resonances detected in Figure 6b. Such detailed information on the different oxygen environments is expected to be of high interest for proposing realistic models of the anatase surface recovered after the milling step, by combining computational modeling to ab initio calculations of the ^{17}O NMR parameters, and comparing the results to experimental ^{17}O NMR data, as previously proposed for other studies on titania surfaces.[9,44]

In summary, although the overall structure of anatase appears to be maintained according to XRD, the texture of the material is affected by the milling process, and ^{17}O NMR further shows that this phase reacts with labeled water to form enriched anatase-like *OTi$_3$ environments after only 1 min of milling. However, in contrast to alumina, only a very small number of labeled *OH species were observed in the 1D ^{17}O MAS NMR spectra (even upon analysis of freshly recovered samples), and these could only be clearly detected using DNP−SENS analyses.

Silica and Zirconia. Preliminary investigations were also performed at different milling times on silica and zirconia. For the former (Figure 7a), characterizations after only 1 min of milling suggested the presence of both silanols (Si-*OH) and siloxanes (Si-*O-Si). The significant proportion of siloxane bridges after 1 min of milling is particularly noteworthy because it demonstrates that the condensation reactions of intermediate Si*OH groups proceeds quickly under the reaction conditions used here. In contrast, in the case of zirconia, it was found that the ^{17}O enrichment using LAG is much more challenging to achieve. Indeed, the two resonances characteristic of the monoclinic form were barely visible after 15 min of milling (Figure 7b). Moreover, no direct evidence of Zr-*OH groups could be detected by conventional ^{17}O NMR (with these being expected around ~100 ppm).[10] The underlying resonances observed as a shoulder around 400 ppm after 1 h of milling may be due to more disordered *OZr$_x$ environments. Further investigations are currently in progress on these phases, from both the synthesis and NMR/DNP points of view, in order to better characterize and control the nature of enriched *OM$_x$ and M-*OH groups at different milling times and to establish the optimal conditions for isotopic labeling.

^{17}O Labeling of Mixtures of Oxides: From Liquid to Solid Oxygen-Transfer Reactions. Having demonstrated that it is possible to perform the direct ^{17}O enrichment of

https://dx.doi.org/10.1021/acs.inorgchem.0c00208
Inorg. Chem. 2020, 59, 13050−13066

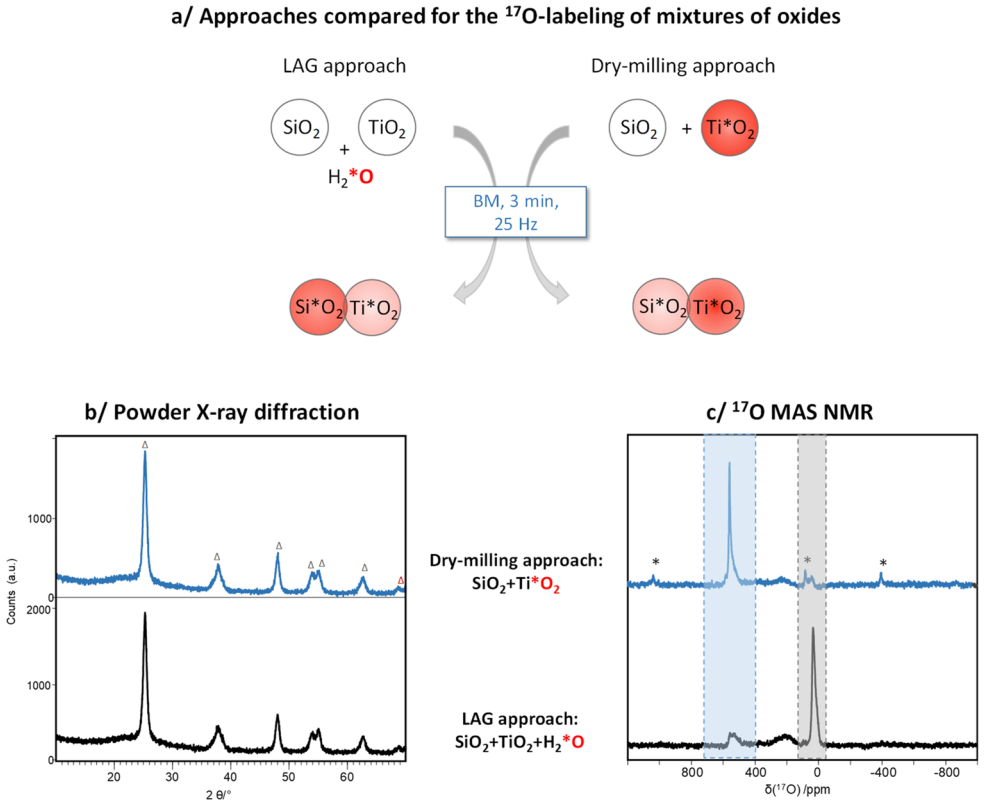

Figure 8. (a) Schematic representation of the two synthetic approaches tested for enriching mixtures of SiO_2 and TiO_2 in ^{17}O using mechanochemistry (shades of red are used to reflect the average relative ^{17}O labeling of the oxides after milling). (b and c) Characterizations of ^{17}O-enriched SiO_2/TiO_2 mixtures using PXRD and solid-state ^{17}O MAS NMR at 20 T. Top: Dry-milling of nonlabeled SiO_2 with enriched Ti^*O_2 for 3 min (blue curves). Bottom: LAG of a mixture of TiO_2 and SiO_2 for 3 min in the presence of $H_2{}^*O$ (black curves). The symbols △ correspond to the diffraction peaks of anatase in PXRD (ICSD 7206075), and the symbols * correspond to spinning sidebands in ^{17}O NMR. The shaded regions on the ^{17}O MAS NMR spectra correspond to the chemical shifts expected for OTi_x (light blue) and siloxane (light gray) environments. An expansion of the ^{17}O NMR spectra in the siloxane region can be found in Figure S14.

simple oxides using LAG, the obvious next step was to see how mechanochemistry can be used to synthesize ^{17}O-labeled *mixed* oxides. Two mechanochemical approaches were considered to introduce the ^{17}O label (Figure 8a): (i) milling the nonlabeled oxide precursors together with $H_2{}^*O$ or (ii) separately preenriching oxide precursors before "dry"-milling them together. While the former strategy was recently used for enriching lithium-ion-battery electrode materials like Li_2RuO_3,[7] no ^{17}O NMR analysis of the milling medium just after the LAG step was reported. Moreover, comparing the two strategies may actually shed light on how oxides react with each other in the solid state during mechanochemical reactions.

These two approaches were tested on a TiO_2/SiO_2 mixture, using the same oxide sources as those mentioned previously (mesoporous anatase and amorphous silica), with the aim of comparing the media recovered just after the milling step, i.e., before any further heat treatment. On the one hand, equimolar quantities of TiO_2 and SiO_2 were milled together by LAG using $H_2{}^*O$. On the other hand, a preenriched Ti^*O_2 phase was dry-milled in the presence of an equimolar quantity of nonlabeled SiO_2. Both media were compared after 3 min of BM. Although the XRD patterns were found to be the same (Figure 8b), their solid-state NMR spectra were completely different (Figure 8c).

In the LAG case, the ^{17}O signatures of enriched titania and silica were both visible but with a significant discrepancy in their relative enrichment, with the vast majority of the isotopic label having entered the silica phase (Figure 8c, black curve). Interestingly, in addition to the $^*OTi_3$ and siloxane resonances, it is worth noting that a broad signal is also observed between ~450 and 100 ppm, i.e., in a zone that covers the range expected for $^*OTi_4$, Si-*O-Ti, and Ti-*OH groups.[46,47] The more distinct contribution around ~200 ppm could be indicative of the formation of a small number of Ti-*OH groups under these synthetic conditions.

In the Ti^*O_2/SiO_2 "dry-milling" case, although the $^*OTi_3$ anatase signal is still predominant, a broad signal is also detected between ~450 and 100 ppm, along with a new resonance around ~30 ppm (Figure 8c, red curve). The latter resonance can be assigned to enriched Si-*O-Si bridges (see Figure S14 for an expansion into the siloxane region). Given that the silica precursor was initially nonlabeled, this clearly points to the fact that the reactions occurring at the interface of Ti^*O_2 and SiO_2 during the BM eventually result in bonding rearrangements around the oxygen atoms, which lead to the enrichment of the silica phase. More importantly, such an "oxygen transfer" between the two oxides starts to occur after just 3 min, meaning that very short milling times are sufficient to mix the reagents intimately, so that they can start reacting at their interface.

The comparison of the two ^{17}O-labeling approaches points to the major advantages of ^{17}O NMR for studying the reactivity of inorganic oxides in BM and helps to understand

https://dx.doi.org/10.1021/acs.inorgchem.0c00208
Inorg. Chem. 2020, 59, 13050−13066

better the differences in reactivity of oxides during BM. On the one hand, it allows identification of the different oxygen environments present, thereby revealing oxygen bonding rearrangements that occur at the interfaces between the oxides. On the other hand, it can also bring clear evidence of discrepancies in the oxygen isotopic distribution within samples. Moreover, the $H_2{}^{17}O$-LAG approach used here could more generally help to shed light on the differences in reactivity of liquid grinding assistants like water with respect to the different components of a mixture, a feature that has not been looked into so far.

Discussion. *New ^{17}O-Enrichment Approaches for Oxides.* The enrichment strategies described above significantly broaden the scope of approaches available for producing ^{17}O-enriched s-, p-, and d-block oxides and offer synthetic alternatives that are highly efficient, in terms of both cost and practicality. One of the reasons for this comes from the nature of the precursors involved: oxides and ^{17}O-enriched water. Oxides are indeed very interesting starting materials either because they are directly commercially available (as for TiO_2, SiO_2, Al_2O_3, and ZrO_2) or because they can be easily produced by the heat treatment of hydroxides (as illustrated here for CaO and Li_2O) or even carbonates. Moreover, being able to perform ^{17}O labeling on commercially available sources of titania, silica, alumina, and zirconia, which can be stored and handled under ambient conditions for several months, is a key advantage in comparison to other procedures used so far for enriching these phases, in which more sensitive alkoxide or chloride precursors had been used.[12−15,46,48−51] Indeed, no safety hazard was involved here in the LAG step that could be easily scaled up to produce gram quantities of labeled material, which contrasts with syntheses involving highly reactive and toxic reagents such as $SiCl_4$ and $TiCl_4$. Although the maximum ^{17}O enrichment is meant to be higher in the latter case (because the only source of oxygen is ^{17}O-enriched water), the ^{17}O content of the phases recovered after LAG was, nevertheless, sufficient for performing a wide range of high-resolution NMR experiments, as shown in the case of the 2D $^1H-^{17}O$ and $^{27}Al-^{17}O$ MAS NMR experiments performed on alumina (Figure 4a−c). Moreover, it is expected that further optimizations of the LAG step could lead to higher enrichments than those achieved so far, by increasing the amount of $H_2{}^*O$ added, varying the texture/porosity of the oxide precursor used, and/or optimizing the BM conditions. Indeed, a preliminary investigation on the ^{17}O labeling of monoclinic zirconia phases of different initial crystallinities was performed, showing the importance of the choice of a precursor on the efficiency of the isotopic enrichment (Figure S15).

Using stoichiometric amounts of ^{17}O-enriched water for the labeling step is also much less hazardous and constraining than having to manipulate ^{17}O-enriched O_2 gas at high temperatures, as had been described in previous ^{17}O-enrichment protocols for oxides.[9,10,12,52] Indeed, labeling reactions were performed here under ambient temperature and pressure and proceeded extremely quickly (less than 1 h of milling). Moreover, in terms of cost, all syntheses were relatively cheap, amounting to less than ∼40 euros for enriching ∼50 mg of compound (when using 90% ^{17}O-enriched water in the syntheses). Overall, this implies that these protocols are expected to be accessible to both research and teaching laboratories and to contribute to the development of advanced spectroscopic studies on various oxides (or oxide mixtures), which would require ^{17}O (or ^{18}O) labeling.

Another very attractive feature of the protocols developed here is that the ^{17}O-enriched phases recovered after LAG can be used in multiple ways. First, they can be converted into related oxide phases by performing additional heat treatments under inert conditions, as illustrated in Figure S16 for alumina and titania. Alternatively, they can directly serve as precursors for the synthesis of more complex mixed-metal oxides, as illustrated in the previous section for the dry-milling of Ti^*O_2 with SiO_2. Last but not least, given that one of the unique properties of the enriched p- and d-block oxides produced here is that they are still mesoporous after LAG, with some of the surface sites enriched in ^{17}O (as suggested by DNP), they could be used as model systems for studying the surface reactivity of oxides by high-resolution ^{17}O NMR. In particular, considering the wide range of applications of transitional aluminas like γ- and δ-Al_2O_3 in heterogeneous catalysis, the ^{17}O-labeled alumina phases prepared by LAG could be of high interest to gain new insight into the surface reactivity of catalytic materials using high-resolution ^{17}O NMR and DNP.

Atomic-Level Insight into Reactions Occurring during BM. Beyond the production of ^{17}O-enriched materials, our results also show how high-resolution ^{17}O NMR and DNP can help to gain atomic-level information into LAG processes and more generally reaction mechanisms in BM. Mechanochemical reactions are indeed far from trivial because they involve both physical steps (mixing of reagents, particle size reduction, creation of reactive surfaces, diffusion of atoms/molecules at the interfaces, etc.) and chemical steps (chemical reactions), both of which are important for the system to evolve toward a given product.[53,54] Despite numerous investigations, some of which include in situ measurements and/or innovative designs of the milling equipment,[54−59] many blind spots remain regarding both the physics and chemistry of mechanochemical reactions. This is even more true when common techniques like XRD are not informative, as observed here for the four p- and d-block oxides, as well as for the mixed SiO_2/TiO_2 system.

In the case of titania, alumina, and silica, ^{17}O NMR and DNP measurements at different milling times were able to provide clear evidence of the presence of intermediate M-*OH species, which can then condense to form $*OM_x$ sites. One important point arising from these analyses was that the quantity of M-*OH sites detected differed significantly from one oxide to the other. In particular, at the shortest milling times, while Al-*OH and Si-*OH groups could be clearly observed, this was not the case for Ti-*OH species, for which DNP analyses were needed to bring evidence of their presence. Given that several parameters can influence the formation of M-*OH groups (the initial degree of covalency or ionicity of the M−O bonds within the oxide, texture, and surface area of the material and reactivity under the BM conditions used), further investigations will be needed to determine the mechanism(s) by which enriched M-*OH groups form for each phase, i.e., whether it is by surface hydrolysis, dissociative adsorption of water, or exchange of labile M-OH groups initially present at the surface. From a more practical perspective, the differences in reactivity shown here demonstrate that milling conditions need to be optimized case by case for each oxide, in order to find how to achieve the highest ^{17}O enrichment possible.

On the basis of the different high-resolution NMR experiments and the changes in porosity observed by N_2

https://dx.doi.org/10.1021/acs.inorgchem.0c00208
Inorg. Chem. 2020, 59, 13050−13066

volumetric analyses, it is reasonable to say that the initial formation of bulklike *OM_x environments by BM under ambient conditions results from the condensation of (transient) M-*OH sites. Because of these surface-reconstruction processes, which lead to changes in some of the oxygen bonds of the initial particles, some enriched oxygen sites that were located at the surface of the oxide particles may become more "core-like". Under a given set of milling conditions, the extent of formation of these *OM_x sites and the depth of enrichment of the initial oxide particles depend on the nature and texture of the initial oxide and the capacity of mechanochemistry to create "fresh" reactive surfaces to trigger these reactions.[53] This is illustrated when comparing the ^{17}O MAS NMR data and SIMS analyses of SiO_2 and TiO_2 and even more so when considering the different ^{17}O NMR analyses of Al_2O_3, as detailed below.

Concerning alumina, solid-state NMR analyses enabled us to shed light on additional features of BM reactions. First, as shown in Figure 3b, it is interesting to note that no "induction time" in the formation of *OAl_x species could be detected within the time scale investigated. Induction periods in BM are generally made evident using XRD techniques,[60−62] but such analyses would have led to an erroneous conclusion here, given that essentially no change was observed in PXRD. Moreover, it is interesting to note that while an increase in the relative number of *OAl_x environments with time was observed, it progressively slowed down after the first 15 min. Given that Al-*OH and *OAl_x environments very easily formed during the milling (because they were detected after only 5 min of reaction), this suggests that other rate-limiting steps take over after 15 min. It is possible that the enrichment of *OAl_x sites then proceeds by other mechanisms, involving the gradual rearrangement of oxygen-bonding environments within the intermediate oxyhydroxy phase. Alternatively, changes in the texture and rheological properties of the medium (due to the progressive consumption of enriched water and/or modification of the mesoporosity of the material) may render the milling process less efficient in creating new reactive surfaces, thereby slowing the speed of enrichment. To go one step further, additional high-resolution ^{17}O NMR and DNP analyses will be needed to study the relative binding of oxygen atoms to Al^{IV} and Al^{VI} sites as a function of the milling time, and the reactivity of the different surface *OH groups created by LAG. This should, in return, help rationalize the enrichment process at the atomic level and better control the nature and proportion between the enriched sites.

Finally, studies on the mixed SiO_2/TiO_2 system show how ^{17}O NMR can be used for looking at reactions occurring at the *interfaces* between different oxides during BM. Indeed, the ^{17}O NMR characterization performed on the {SiO_2 + Ti*O_2} system demonstrates that, after only 3 min of reaction, a variety of ^{17}O-enriched oxygen environments are present, which include enriched oxygen atoms within the silica phase. Being able to provide such atomic-level insight at the very early stages of the reaction is important to evaluate the efficiency of a given milling process to mix different solid particles (whether they are crystalline or amorphous, as is the case here) and to create contacts between them that will allow solid/solid reactions to occur. More generally, such analyses will certainly help to understand better what *chemical* reactions occur during BM when disordered or amorphous phases are involved, with such reactions being intrinsically very complex to study.

CONCLUSION

In this manuscript, we have shown how the ^{17}O labeling of oxides using mechanochemistry can be used for two main purposes: (i) preparing ^{17}O-enriched oxides and (ii) understanding reaction mechanisms occurring during BM. Concerning the first point, LAG in the presence of ^{17}O-enriched water was shown to be a highly attractive enrichment strategy for the fast and straightforward labeling of simple oxides of the s, p, and d blocks, starting from the nonlabeled oxide precursors. Regarding the second point, it was demonstrated how, thanks to mechanochemistry-mediated isotopic labeling, it becomes possible to address questions regarding the physical and chemical processes occurring at the atomic level during BM, by performing advanced solid-state ^{17}O NMR analyses, including ultrahigh-field NMR, DNP, and fast MAS measurements. In this context, one of the highlights of this work is to shed light on what chemical reactions start to occur at the interfaces between different oxide particles in the first few minutes of milling. Given that milling together inorganic precursors is frequently one of the first steps in the synthesis of functional mixed-metal oxides, performing similar high-resolution ^{17}O NMR analyses on different mixtures of enriched oxide precursors and under different milling conditions could not only help to optimize the milling process but also help to identify intermediate phases, which could, in turn, serve for the preparation of novel materials.

EXPERIMENTAL SECTION

Synthesis of ^{17}O-Labeled Phases. *Reagents and Milling Equipment.* Calcium hydroxide [$Ca(OH)_2$, Sigma-Aldrich, ≥96%] and lithium hydroxide monohydrate ($LiOH·H_2O$, Prolabo Normapur, Analytical Reagent, ≥99.0%) were used as received and served as precursors for the synthesis of CaO and Li_2O. Silica (SiO_2, Aerosil 200, Degussa, 180 m^2/g), alumina (Al_2O_3, "aluminoxid C", Degussa, mixture of γ and δ forms, 100 m^2/g), titania (TiO_2, St-Gobain Norpro, anatase phase, 150 m^2/g), and zirconia (ZrO_2, St-Gobain Norpro, monoclinic form, 85 m^2/g) were dried under vacuum for 3 to 4 h at room temperature prior to use. ^{17}O-labeled water (with 40% or 90% ^{17}O enrichment) was purchased from CortecNet. ^{18}O-labeled water (with 97% ^{18}O enrichment) was purchased from Eurisotop. For DNP experiments, TEKPol[63] was purchased from Cortecnet.

All milling treatments were carried out at ∼22 °C (±3 °C) in a Retsch Mixer Mill 400 apparatus, using 10 mL stainless steel grinding jars with screwtop or push-fit lids. Unless otherwise noted, the protocols were first tested in triplicate using non-labeled water, before being performed with ^{17}O (or ^{18}O)-enriched water.

*Synthesis of Ca(*OH)$_2$ and Ca*O.* Nonlabeled $Ca(OH)_2$ was first heat-treated to 950 °C in a tubular furnace under an argon atmosphere (heating rate, 10 °C/min; dwell time at 950 °C, 4 h) to produce CaO. The freshly prepared CaO phase (50 mg, 0.9 mmol, 1 equiv) was introduced into a grinding jar, together with 16 μL of 40%-enriched $H_2{}^{17}O$ (0.9 mmol, 1 equiv) with two stainless steel balls (10 mm diameter). The jar was closed and subjected to grinding for 1 h in the mixer mill operated at 25 Hz. The reactor was opened, and the white powder, which progressively dries upon contact with air, was recovered by scraping the edges of the reactor and beads with a spatula and characterized by XRD and solid-state ^{17}O NMR, showing the formation of $Ca(*OH)_2$ [average yield (n = 4): 54 mg, 82%]. ^{17}O-enriched CaO was then synthesized by heat treatment of the labeled hydroxide for 4 h at 950 °C in a tubular furnace under an argon atmosphere, using the same conditions as those above.

LAG of SiO$_2$. SiO_2 (50 mg, 0.84 mmol, 1.0 equiv) was introduced into a screwtop grinding jar with ^{17}O-labeled water (15 μL, 0.83 mmol, 1.0 equiv) and two stainless steel balls (10 mm diameter). The jar was closed and subjected to grinding for milling times ranging from 1 min to 1 h in a mixer mill operated at 25 Hz. The reactor was

https://dx.doi.org/10.1021/acs.inorgchem.0c00208
Inorg. Chem. 2020, 59, 13050−13066

opened, and the sample was recovered by scraping the edges of the reactor and beads with a spatula [average mass of the crude material (n = 4): 60 mg]. The recovered sample was white for short milling times but light gray beyond 15 min of milling (see Figure S2 for EDXS analyses). Samples were then dried under vacuum at room temperature.

LAG of Al_2O_3. Al_2O_3 (50 mg, 0.49 mmol, 1.0 equiv) was introduced into a grinding jar with ^{17}O-labeled water (13 μL, 0.72 mmol, 1.5 equiv) and one stainless steel ball (10 mm diameter). The jar was closed and subjected to grinding for milling times ranging from 5 min to 1 h in a mixer mill operated at 25 Hz. The reactor was opened, and the solid powder was recovered by scraping the edges of the reactor and beads with a spatula [average mass of the crude material (n = 4): 45 mg]. The recovered sample was white for short milling times but very light gray beyond 15 min of milling (see Figure S3 for EDXS analyses). Depending on the sample, further treatments were performed either under vacuum at room temperature or at high temperature under an argon atmosphere (heating rate, 10 °C/min; dwell time at 900 °C, 4 h; Figure S16).

LAG of TiO_2. TiO_2 (50 mg, 0.63 mmol, 1.0 equiv) was introduced into a grinding jar with ^{17}O-labeled water (11 μL, 0.61 mmol, 1.0 equiv) and one stainless steel ball (10 mm diameter). The jar was closed and subjected to grinding for milling times ranging from 1 min to 1 h in a mixer mill operated at 25 Hz. The reactor was opened, and the solid powder was recovered by scraping the edges of the reactor and beads with a spatula [average mass of the crude material (n = 4): 44 mg]. The recovered sample was white for short milling times but light gray/yellowish beyond 15 min of milling (see Figure S4 for EDXS analyses). Depending on the sample, further treatments were performed, either under vacuum at room temperature or at high temperature under an argon atmosphere (heating rate, 10 °C/min; dwell time at 900 °C, 4 h; Figure S16).

LAG of ZrO_2. ZrO_2 (50 mg, 0.41 mmol, 1 equiv) was introduced into a grinding jar with ^{17}O-labeled water (7 μL, 0.39 mmol, 1 equiv) and one stainless steel ball (10 mm diameter). The jar was closed and subjected to grinding for milling times ranging from 15 min to 1 h in a mixer mill operated at 25 Hz. The reactor was opened, and the solid powder was recovered by scraping the edges of the reactor and beads with a spatula [average mass of the crude material (n = 4): 42 mg]. The recovered sample was white for short milling times but very light gray beyond 15 min of milling (see Figure S5 for EDXS analyses). Samples were then dried under vacuum at room temperature.

LAG of TiO_2 and SiO_2. TiO_2 (28.3 mg, 0.35 mmol, 1 equiv) and SiO_2 (21.5 mg, 0.35 mmol, 1 equiv) were introduced into a grinding jar with ^{17}O-labeled water (13 μL, 0.72 mmol, 2 equiv) and one stainless steel ball (10 mm diameter). The jar was closed and subjected to grinding for 3 min in a mixer mill operated at 25 Hz. The reactor was opened, and the white powder was recovered by scraping the edges of the reactor and beads (m ∼ 43 mg).

BM of TiO_2 with SiO_2.* Ti*O_2 was first synthesized as described above, by milling TiO_2 for 15 min and then drying the sample under vacuum for 1 h at room temperature. Then, labeled Ti*O_2 (28.6 mg, ∼0.35 mmol, 1 equiv) was introduced into a grinding jar with nonlabeled SiO_2 (21.4 mg, 0.35 mmol, 1 equiv) and one stainless steel ball (10 mm diameter). The jar was closed and subjected to grinding for 3 min in a mixer mill operated at 25 Hz. The reactor was opened, and the solid powder was recovered by scraping the edges of the reactor and beads (m = 42 mg).

Characterization Techniques. *PXRD.* PXRD analyses were carried out on a Philips X'pert Pro MPD diffractometer using Cu Kα_1 radiation (λ = 1.5406 Å) in a Bragg−Brentano scanning mode with a 2θ angle between 10 and 70° and a time per step ranging from of 30 to 240 s, depending on the sample.

SEM and EDXS Analyses. SEM measurements were conducted on a Hitachi S4800 instrument under an excitation voltage between 0.5 and 8.0 kV depending on each powder's surface charging. For SEM, powdered samples were deposited on double-sided conducting carbon tape and then platinum-metallized by sputtering under vacuum. EDXS analyses were carried out on a Zeiss Evo HD15 scanning electron microscope equipped with an Oxford Instruments X-MaxN SDD 50 mm^2 EDXS detector. For EDXS, powdered samples were deposited on double-sided conducting carbon tape and then metallized with carbon before analyses.

N_2 Adsorption/Desorption Isotherms. N_2 volumetric analyses were performed by physisorption of N_2 using a Tristar instrument (Micromeritics, Norcross, GA). Prior to measurements, samples were degassed under vacuum overnight at 150 °C.

SIMS. SIMS analyses were performed on (i) SiO_2 and TiO_2 samples that had been enriched by LAG as described previously (1 h of BM) but using 97% ^{18}O-labeled water and (ii) nonlabeled SiO_2 and TiO_2 phases, which served as controls. All samples were pelletized, dried under vacuum, and then sputtered by a thin layer of gold prior to analysis. Measurements were performed on the IMS4F apparatus (Cameca) of the Geosciences Platform of the University of Montpellier, equipped with a 10 keV cesium sputter gun. For each sample, average ^{18}O/^{16}O ratios were determined by analyzing three different zones of the surface and performing five blocks of 10 measurements on each zone.

Solid-State ^{17}O NMR 1D Experiments. The majority of solid-state ^{17}O NMR experiments were performed on a Varian VNMRS 600 MHz (14.1 T) NMR spectrometer, using either Varian 3.2 mm HX or HXY probes or a Phoenix 3.2 mm probe, tuned to ^{1}H (599.82 MHz) and ^{17}O (81.31 MHz). Spectra were recorded under MAS conditions, with spinning speeds ranging from 16 to 20 kHz, depending on the sample. Additional ^{17}O MAS NMR experiments were performed on a Bruker 850 MHz (20.0 T) NMR spectrometer, using Bruker 1.3 or 3.2 mm probes, tuned to ^{1}H (850.23 MHz) and ^{17}O (115.26 MHz). Finally, ultrahigh-magnetic-field experiments were also performed on the 1.5 GHz (35.2 T) SCH instrument in Tallahassee, FL,[64] using a 3.2 mm single-channel MAS probe, spinning at 18 kHz. The acquisition parameters used for each sample can be found in Table S1. ^{17}O-enriched Ca(*OH)$_2$ was used to set up the DFS enhancement scheme[65] and ^{17}O{^{1}H} CPMAS NMR experiments. ^{17}O chemical shifts were referenced externally to tap water at 0.0 ppm (or to D_2O at −2.7 ppm).

Solid-State ^{27}Al NMR 1D Experiments. Solid-state ^{27}Al NMR experiments were performed on a Varian VNMRS 600 MHz (14.1 T) NMR spectrometer, using a Varian 3.2 mm HX probe or a Phoenix 3.2 mm probe, tuned to ^{1}H (599.82 MHz) and ^{27}Al (156.29 MHz). Samples were packed into low-aluminum background zirconia rotors for these measurements. Single-pulse experiments were performed by spinning at 18 kHz, using a ^{27}Al excitation pulse of 0.7 μs (π/18 tip angle) and a recycle delay of 6 s, and acquiring a total of 512 transients. ^{27}Al{^{1}H} CPMAS NMR experiments were performed by spinning at 18 kHz, using a ^{1}H excitation pulse of 6 μs (π/2 tip angle) and a contact time of 0.5 ms. The recycle delay was set to 1 s, and the number of scans acquired ranged from 8000 to 61700, depending on the sample. ^{27}Al chemical shifts were referenced externally to a 1 M aqueous solution of $Al(NO_3)_3$.

Solid-State ^{1}H NMR 1D Experiments. Solid-state ^{1}H fast MAS NMR spectra were recorded on a Bruker 850 MHz (20.0 T) instrument, using a Bruker 1.3 mm probe spinning at 60 kHz. A Hahn-echo sequence was used, with π/2 and π pulses of 2.05 and 4.1 μs, and a rotor-synchronized echo delay corresponding to 2 or 50 rotor periods (Figure 4d). ^{1}H chemical shifts were referenced to a dipeptide (Asp-Ala), used as a secondary reference, with the low-frequency signal being set to 1.1 ppm with respect to tetramethylsilane. Additional Hahn-echo ^{1}H NMR spectra were also recorded on a Varian VNMRS 600 MHz (14.1 T) NMR spectrometer using a Phoenix 1.2 mm MAS probe, in order to evaluate the potential contributions of background ^{1}H signals from the rotor and caps (Figure S10).

^{27}Al{^{17}O} J-HMQC NMR. A ^{27}Al{^{17}O} J-HMQC MAS NMR experiment was performed on a Bruker 850 MHz (20.0 T) NMR spectrometer, using a 3.2 mm HXY probe, tuned to ^{1}H (850.29 MHz), ^{27}Al (221.56 MHz), and ^{17}O (115.27 MHz), and spinning at 24 kHz. DFS excitation pulses were first applied on ^{27}Al (1 ms pulse of 30 W with a 600 to 150 kHz sweep). The π/2 and π pulses on ^{27}Al were set to 8.3 and 16.6 μs, respectively [∼10 kHz radio frequency (RF)]. The evolution delay following the π/2 pulse on ^{27}Al was set to

https://dx.doi.org/10.1021/acs.inorgchem.0c00208
Inorg. Chem. 2020, 59, 13050−13066

2.5 ms. The $\pi/2$ pulses on ^{17}O were set to 8.5 μs (~10 kHz RF). Spinal-64 ^{1}H decoupling (100 kHz RF) was applied throughout the sequence (except during the DFS). The recycle delay was set to 1 s, and a total of 10000 scans were acquired for each of the 18 increments of the 2D experiments. The ^{17}O and ^{27}Al chemical shifts were referenced using respectively tap water (at 0 ppm) and a 1 mol/L solution of aluminum nitrate (at 0 ppm).

$^{1}H\{^{17}O\}$ D- and J-HMQC NMR. $^{1}H\{^{17}O\}$ HMQC MAS NMR experiments were performed on a Bruker 850 MHz (20.0 T) NMR spectrometer, using a 1.3 mm HX probe, tuned to ^{1}H (850.29 MHz) and ^{17}O (115.27 MHz), and spinning at 60 kHz. The $\pi/2$ and π pulses on ^{1}H were set to 2.05 and 4.1 μs, respectively. The $\pi/2$ pulses on ^{17}O were set to 6.0 μs. For the J-HMQC experiment, the evolution delay following the $\pi/2$ pulse on ^{1}H was set to 600 μs. For the D-HMQC experiment, the recoupling time τ_{rec} was set to 100 or 300 μs, during which an $SR4^2_1$ pulse was applied on ^{1}H (120 kHz RF) and a WURST pulse was applied on ^{17}O (at an offset of 120 kHz).[66] The recycle delay was set to 0.5 s. The number of scans and duration of each experiment can be found in Table S1. ^{17}O and ^{1}H chemical shifts were referenced using respectively tap water (at 0 ppm) and a dipeptide (Asp-Ala), for which the low-frequency signal was set to 1.1 ppm with respect to tetramethylsilane.

^{17}O MQMAS NMR. A ^{17}O MQMAS NMR experiment was performed on an enriched alumina phase on the SCH instrument in Tallahassee, FL,[64] using a 3.2 mm single-channel MAS probe, and spinning at 16 kHz. ^{17}O excitation and conversion pulses were respectively set to 4 and 1.4 μs (600 W power), followed by a 4.4 μs pulse (36 W power). The recycle delay was set to 0.2 s, and a total of 240 scans were acquired for each of the increments of the 2D experiments. ^{17}O chemical shifts were referenced externally to D_2O at −2.7 ppm (which was measured to be equivalent to tap water at 0 ppm).

^{17}O DNP. The MAS DNP experiments were carried out on the 600 MHz/395 GHz setup installed at the NHMFL in Tallahassee, FL. The magnetic field was set at 14.094 T, and the gyrotron generates a microwave power of 12 W at the probe base and a frequency of 395.166 GHz. The sample was packed in a 3.2 mm thin-wall ZrO_2 rotor and spun at 13 kHz. The temperatures for VT/bearing/drive were 91.6/98/110 K, leading to a sample temperature under microwave irradiation of ~100 K and ~94 K in the absence of it.[38] The higher drive temperature allowed us to achieve a 13 kHz spinning frequency while reducing the pressure needed. The sample was prespun at room temperature with a benchtop spinner (home-built), and electron paramagnetic resonance measurement was carried out prior to the MAS DNP experiment. Finally, three freeze−thaw cycles were applied to the sample before insertion into the probe. The powder was impregnated with a 16 mM solution of TEKPol (purchased from Cortecnet) in tetrachloroethane-d_2 (Cortecnet) for Al_2O_3 or tetrabromoethane (Sigma-Aldrich) for TiO_2. For the experiments, ~30 mg of powder was impregnated with ~30 μL of solution, leading to a toothpasty texture. The NMR acquisition parameters used for each spectrum are reported in Table S1 for the $^{17}O\{^{1}H\}$ CPMAS NMR and DFS-echo experiments performed with or without microwaves.

■ ASSOCIATED CONTENT

Supporting Information

The Supporting Information is available free of charge at https://pubs.acs.org/doi/10.1021/acs.inorgchem.0c00208.

Preliminary study on the synthesis of ^{17}O-enriched $Li_2{}^*O$ (including Figure S1); SEM, N_2 adsorption/desorption isotherms, and EDXS analyses of SiO_2 (Figure S2), Al_2O_3 (Figure S3), TiO_2 (Figure S4), and ZrO_2 (Figure S5); ^{17}O MAS NMR spectra of enriched $Zr{}^*O_2$ and the empty zirconia rotor (Figure S6a) and a non-labeled Al_2O_3 phase (Figure S6b); fit of the ^{17}O MAS NMR spectrum of enriched $Si{}^*O_2$ recovered after 1 h of BM (Figure S7); ^{27}Al MAS and $^{27}Al\{^{1}H\}$ CPMAS NMR analyses of Al_2O_3 phases before and after enrichment (Figure S8); fits of ^{17}O MAS NMR spectra of enriched $Al_2{}^*O_3$ after different milling times (Figure S9); fast MAS ^{1}H NMR spectra of enriched $Al_2{}^*O_3$ and comparison to the rotor ^{1}H background signal (Figure S10); ^{17}O DNP and $^{17}O\{^{1}H\}$ DNP CPMAS NMR spectra of enriched $Al_2{}^*O_3$ (Figure S11); ^{17}O MAS and $^{17}O\{^{1}H\}$ CPMAS NMR spectra of enriched $Al_2{}^*O_3$ (Figure S12); fit of the ^{17}O MAS NMR spectrum of enriched $Si{}^*O_2$ recovered after 1 min of BM (Figure S13); analysis of the siloxane region of ^{17}O MAS NMR spectra of SiO_2/TiO_2 mixtures labeled using different procedures (Figure S14); ^{17}O MAS NMR spectra of zirconia phases of different initial crystallinity recovered after 1 h of BM (Figure S15); ^{17}O MAS NMR spectra of enriched alumina and titania after heat treatment at 900 °C (Figure S16); and ^{17}O NMR parameters used for acquisition of the NMR spectra (Table S1) (PDF)

■ AUTHOR INFORMATION

Corresponding Author

Danielle Laurencin − *ICGM, Univ. Montpellier, CNRS, ENSCM, Montpellier 34090, France;* orcid.org/0000-0002-7445-0528; Email: danielle.laurencin@umontpellier.fr

Authors

Chia-Hsin Chen − *ICGM, Univ. Montpellier, CNRS, ENSCM, Montpellier 34090, France;* orcid.org/0000-0001-5151-1765

Emeline Gaillard − *ICGM, Univ. Montpellier, CNRS, ENSCM, Montpellier 34090, France*

Frédéric Mentink-Vigier − *National High Magnetic Field Laboratory (NHMFL), Florida State University, Tallahassee, Florida 32306, United States;* orcid.org/0000-0002-3570-9787

Kuizhi Chen − *National High Magnetic Field Laboratory (NHMFL), Florida State University, Tallahassee, Florida 32306, United States*

Zhehong Gan − *National High Magnetic Field Laboratory (NHMFL), Florida State University, Tallahassee, Florida 32306, United States*

Philippe Gaveau − *ICGM, Univ. Montpellier, CNRS, ENSCM, Montpellier 34090, France*

Bertrand Rebière − *ICGM, Univ. Montpellier, CNRS, ENSCM, Montpellier 34090, France*

Romain Berthelot − *ICGM, Univ. Montpellier, CNRS, ENSCM, Montpellier 34090, France;* orcid.org/0000-0003-1534-2663

Pierre Florian − *Conditions Extrêmes et Matériaux: Haute Température et Irradiation (CEMHTI), UPR 3079, CNRS, Université d'Orléans, 45071 Orléans, France*

Christian Bonhomme − *Laboratoire de Chimie de la Matière Condensée de Paris, UMR 7574, CNRS, Sorbonne Université, Paris 75005, France;* orcid.org/0000-0003-0802-6961

Mark E. Smith − *Vice-Chancellor's Office, Highfield Campus, University of Southampton, Southampton SO17 1BJ, U.K.; Department of Chemistry, Lancaster University, Bailrigg, Lancaster LA1 4YB, U.K.;* orcid.org/0000-0002-6254-6792

Thomas-Xavier Métro − *IBMM, Univ. Montpellier, CNRS, ENSCM, Montpellier 34090, France;* orcid.org/0000-0003-2280-3595

https://dx.doi.org/10.1021/acs.inorgchem.0c00208
Inorg. Chem. 2020, 59, 13050−13066

Bruno Alonso − *ICGM, Univ. Montpellier, CNRS, ENSCM, Montpellier 34090, France;* orcid.org/0000-0002-3430-1931

Complete contact information is available at: https://pubs.acs.org/10.1021/acs.inorgchem.0c00208

Author Contributions

C.-H.C., E.G., R.B., B.R., T.-X.M., and D.L. participated in the synthesis and characterization of the enriched materials. C.-H.C., P.G., B.A., and D.L. performed SSNMR analyses at 14.1 T. F.M.-V. carried out all DNP experiments. K.C., Z.G., P.F., C.B., M.E.S., B.A., and D.L. participated in the ultrahigh-field NMR experiments. C.-H.C., T.-X.M., B.A., and D.L. designed the investigations, and D.L. coordinated the project. All coauthors participated in the writing of the manuscript.

Notes

The authors declare no competing financial interest.

■ ACKNOWLEDGMENTS

This project has received funding from the European Research Council (ERC) under the European Union's Horizon 2020 research and innovation program (Grant 772204; 2017 ERC−COG, MISOTOP project). A portion of this work was performed at the NHMFL, which is supported by the National Science Foundation Cooperative Agreement DMR-1644779, the State of Florida, and the United States Department of Energy. The MAS-DNP system at the NHMFL is funded in part by Grants NIH S10 OD018519 and P41 GM122698. Financial support from the IR-RMN-THC Fr3050 CNRS for conducting part of the high-field NMR experiments is gratefully acknowledged. The UK 850 MHz solid-state NMR facility used in this research was funded by EPSRC and BBSRC, as well as the University of Warwick including via part funding through Birmingham Science City Advanced Materials Projects 1 and 2 supported by Advantage West Midlands and the European Regional Development Fund. Dr. Franck Fayon (CEMHTI, CNRS) and Dr. Dinu Iuga (University of Warwick) are acknowledged for discussions and Anastasia Kuznetsova for the BM enrichment of some of the alumina phases studied here.

■ REFERENCES

(1) Ashbrook, S. E.; Smith, M. E. Solid state ^{17}O NMR—an introduction to the background principles and applications to inorganic materials. *Chem. Soc. Rev.* **2006**, *35*, 718−735.

(2) Huo, H.; Peng, L.; Gan, Z.; Grey, C. P. Solid-State MAS NMR Studies of Brønsted Acid Sites in Zeolite H-Mordenite. *J. Am. Chem. Soc.* **2012**, *134*, 9708−9720.

(3) Bignami, G. P. M.; Davis, Z. H.; Dawson, D. M.; Morris, S. A.; Russell, S. E.; McKay, D.; Parke, R. E.; Iuga, D.; Morris, R. E.; Ashbrook, S. E. Cost-effective ^{17}O enrichment and NMR spectroscopy of mixed-metal terephthalate metal−organic frameworks. *Chem. Sci.* **2018**, *9*, 850−859.

(4) Bignami, G. P. M.; Dawson, D. M.; Seymour, V. R.; Wheatley, P. S.; Morris, R. E.; Ashbrook, S. E. Synthesis, Isotopic Enrichment, and Solid-State NMR Characterization of Zeolites Derived from the Assembly, Disassembly, Organization, Reassembly Process. *J. Am. Chem. Soc.* **2017**, *139*, 5140−5148.

(5) Heard, C. J.; Grajciar, L.; Rice, C. M.; Pugh, S. M.; Nachtigall, P.; Ashbrook, S. E.; Morris, R. E. Fast room temperature lability of aluminosilicate zeolites. *Nat. Commun.* **2019**, *10*, 4690.

(6) Reeves, P. J.; Seymour, I. D.; Griffith, K. J.; Grey, C. P. Characterizing the Structure and Phase Transition of Li_2RuO_3 Using Variable-Temperature ^{17}O and ^{7}Li NMR Spectroscopy. *Chem. Mater.* **2019**, *31*, 2814−2821.

(7) Geng, F.; Shen, M.; Hu, B.; Liu, Y.; Zeng, L.; Hu, B. Monitoring the evolution of local oxygen environments during $LiCoO_2$ charging via ex situ ^{17}O NMR. *Chem. Commun.* **2019**, *55*, 7550−7553.

(8) Hope, M. A.; Halat, D. M.; Magusin, P. C. M. M.; Paul, S.; Peng, L.; Grey, C. P. Surface-selective direct ^{17}O DNP NMR of CeO_2 nanoparticles. *Chem. Commun.* **2017**, *53*, 2142−2145.

(9) Li, Y.; Wu, X.-P.; Jiang, N.; Lin, M.; Shen, L.; Sun, H.; Wang, Y.; Wang, M.; Ke, X.; Yu, Z.; Gao, F.; Dong, L.; Guo, X.; Hou, W.; Ding, W.; Gong, X.-Q.; Grey, C. P.; Peng, L. Distinguishing faceted oxide nanocrystals with ^{17}O solid-state NMR spectroscopy. *Nat. Commun.* **2017**, *8*, 581.

(10) Shen, L.; Wu, X.-P.; Wang, Y.; Wang, M.; Chen, J.; Li, Y.; Huo, H.; Hou, W.; Ding, W.; Gong, X.-Q.; Peng, L. ^{17}O Solid-State NMR Studies of ZrO_2 Nanoparticles. *J. Phys. Chem. C* **2019**, *123*, 4158−4167.

(11) Chen, J.; Wu, X.-P.; Hope, M. A.; Qian, K.; Halat, D. M.; Liu, T.; Li, Y.; Shen, L.; Ke, X.; Wen, Y.; Du, J.-H.; Magusin, P. C. M. M.; Paul, S.; Ding, W.; Gong, X.-Q.; Grey, C. P.; Peng, L. Polar surface structure of oxide nanocrystals revealed with solid-state NMR spectroscopy. *Nat. Commun.* **2019**, *10*, 5420.

(12) MacKenzie, K. J. D.; Smith, M. E. *Multinuclear Solid-State Nuclear Magnetic Resonance of Inorganic Materials*; Pergamon, 2002; Chapter 6.

(13) Jaworski, A.; Stevensson, B.; Edén, M. Direct ^{17}O NMR experimental evidence for Al−NBO bonds in Si-rich and highly polymerized aluminosilicate glasses. *Phys. Chem. Chem. Phys.* **2015**, *17*, 18269−18272.

(14) Bastow, T. J.; Smith, M. E.; Whitfield, H. J. Characterisation of zirconia gels by ^{17}O nuclear magnetic resonance. *J. Mater. Chem.* **1992**, *2*, 989−990.

(15) Bastow, T. J.; Moodie, A. F.; Smith, M. E.; Whitfield, H. J. Characterisation of titania gels by ^{17}O nuclear magnetic resonance and electron diffraction. *J. Mater. Chem.* **1993**, *3*, 697−702.

(16) Babonneau, F.; Bonhomme, C.; Gervais, C.; Maquet, J. Advances in Characterisation Methods for Sol-Gel Derived Materials: High Resolution Solid State Nuclear Magnetic Resonance. *J. Sol-Gel Sci. Technol.* **2004**, *31*, 9−17.

(17) Griffin, J. M.; Clark, L.; Seymour, V. R.; Aldous, D. W.; Dawson, D. M.; Iuga, D.; Morris, R. E.; Ashbrook, S. E. Ionothermal ^{17}O enrichment of oxides using microlitre quantities of labelled water. *Chem. Sci.* **2012**, *3*, 2293−2300.

(18) Métro, T.-X.; Gervais, C.; Martinez, A.; Bonhomme, C.; Laurencin, D. Unleashing the Potential of ^{17}O NMR Spectroscopy Using Mechanochemistry. *Angew. Chem.* **2017**, *129*, 6907−6911.

(19) James, S. L.; Adams, C. J.; Bolm, C.; Braga, D.; Collier, P.; Friščić, T.; Grepioni, F.; Harris, K. D. M.; Hyett, G.; Jones, W.; Krebs, A.; Mack, J.; Maini, L.; Orpen, A. G.; Parkin, I. P.; Shearouse, W. C.; Steed, J. W.; Waddell, D. C. Mechanochemistry: opportunities for new and cleaner synthesis. *Chem. Soc. Rev.* **2012**, *41*, 413−447.

(20) Friščić, T.; Mottillo, C.; Titi, H. M. Mechanochemistry for Synthesis. *Angew. Chem., Int. Ed.* **2020**, *59*, 1018.

(21) Bowmaker, G. A. Solvent-assisted mechanochemistry. *Chem. Commun.* **2013**, *49*, 334−348.

(22) Leskes, M.; Moore, A. J.; Goward, G. R.; Grey, C. P. Monitoring the Electrochemical Processes in the Lithium−Air Battery by Solid State NMR Spectroscopy. *J. Phys. Chem. C* **2013**, *117*, 26929−26939.

(23) Abys, J. A.; Barnes, D. M.; Feller, S.; Rouse, G. B.; Risen, W. M. Preparation of O^{17}-labelled glasses and glass precursers. *Mater. Res. Bull.* **1980**, *15*, 1581−1587.

(24) Merle, N.; Trébosc, J.; Baudouin, A.; Rosal, I. D.; Maron, L.; Szeto, K.; Genelot, M.; Mortreux, A.; Taoufik, M.; Delevoye, L.; Gauvin, R. M. ^{17}O NMR Gives Unprecedented Insights into the Structure of Supported Catalysts and Their Interaction with the Silica Carrier. *J. Am. Chem. Soc.* **2012**, *134*, 9263−9275.

(25) Freude, D.; Haase, J. Survey of NMR Parameters for Quadrupolar Nuclei in Powder Materials. *Particular for ^{27}Al, ^{23}Na and ^{17}O*; 2019; http://www.quad-nmr.de.
(26) Walter, T. H.; Oldfield, E. Magic angle spinning oxygen-17 NMR of aluminum oxides and hydroxides. *J. Phys. Chem.* **1989**, *93*, 6744−6751.
(27) Bastow, T. J.; Stuart, S. N. ^{17}O NMR in simple oxides. *Chem. Phys.* **1990**, *143*, 459−467.
(28) Sun, X.; Dyballa, M.; Yan, J.; Li, L.; Guan, N.; Hunger, M. Solid-state NMR investigation of the $^{16/17}O$ isotope exchange of oxygen species in pure-anatase and mixed-phase TiO_2. *Chem. Phys. Lett.* **2014**, *594*, 34−40.
(29) Pimentel, H. R. X.; Aguiar, D. L. M.; San Gil, R. A. S.; Souza, E. F.; Ferreira, A. R.; Leitão, A. A.; Alencastro, R. B.; Menezes, S. M. C.; Chiaro, S. S. X. ^{17}O MAS NMR and first principles calculations of ZrO_2 polymorphs. *Chem. Phys. Lett.* **2013**, *555*, 96−100.
(30) Li, W.; Wang, Q.; Xu, J.; Aussenac, F.; Qi, G.; Zhao, X.; Gao, P.; Wang, C.; Deng, F. Probing the surface of γ-Al_2O_3 by oxygen-17 dynamic nuclear polarization enhanced solid-state NMR spectroscopy. *Phys. Chem. Chem. Phys.* **2018**, *20*, 17218−17225.
(31) Oglesby, J. V.; Zhao, P.; Stebbins, J. F. Oxygen sites in hydrous aluminosilicate glasses: the role of Al-O-Al and H_2O. *Geochim. Cosmochim. Acta* **2002**, *66*, 291−301.
(32) Neuhoff, P. S.; Zhao, P.; Stebbins, J. F. Effect of extraframework species on ^{17}O NMR chemical shifts in zeolite A. *Microporous Mesoporous Mater.* **2002**, *55*, 239−251.
(33) Frydman, L.; Harwood, J. S. Isotropic Spectra of Half-Integer Quadrupolar Spins from Bidimensional Magic-Angle Spinning NMR. *J. Am. Chem. Soc.* **1995**, *117*, 5367−5368.
(34) Batista, A. T. F.; Wisser, D.; Pigeon, T.; Gajan, D.; Diehl, F.; Rivallan, M.; Catita, L.; Gay, A.-S.; Lesage, A.; Chizallet, C.; Raybaud, P. Beyond γ-Al_2O_3 crystallite surfaces: The hidden features of edges revealed by solid-state ^1H NMR and DFT calculations. *J. Catal.* **2019**, *378*, 140−143.
(35) Pourpoint, F.; Gervais, C.; Bonhomme-Coury, L.; Azaïs, T.; Coelho, C.; Mauri, F.; Alonso, B.; Babonneau, F.; Bonhomme, C. Calcium Phosphates and Hydroxyapatite: Solid-State NMR Experiments and First-Principles Calculations. *Appl. Magn. Reson.* **2007**, *32*, 435−457.
(36) Taoufik, M.; Szeto, K. C.; Merle, N.; Rosal, I. D.; Maron, L.; Trébosc, J.; Tricot, G.; Gauvin, R. M.; Delevoye, L. Heteronuclear NMR Spectroscopy as a Surface-Selective Technique: A Unique Look at the Hydroxyl Groups of γ-Alumina. *Chem. - Eur. J.* **2014**, *20*, 4038−4046.
(37) Digne, M.; Raybaud, P.; Sautet, P.; Guillaume, D.; Toulhoat, H. Atomic Scale Insights on Chlorinated γ-Alumina Surfaces. *J. Am. Chem. Soc.* **2008**, *130*, 11030−11039.
(38) Rossini, A. J.; Zagdoun, A.; Lelli, M.; Lesage, A.; Copéret, C.; Emsley, L. Dynamic Nuclear Polarization Surface Enhanced NMR Spectroscopy. *Acc. Chem. Res.* **2013**, *46*, 1942−1951.
(39) Lesage, A.; Lelli, M.; Gajan, D.; Caporini, M. A.; Vitzthum, V.; Miéville, P.; Alauzun, J.; Roussey, A.; Thieuleux, C.; Mehdi, A.; Bodenhausen, G.; Coperet, C.; Emsley, L. Surface Enhanced NMR Spectroscopy by Dynamic Nuclear Polarization. *J. Am. Chem. Soc.* **2010**, *132*, 15459−15461.
(40) Scolan, E.; Magnenet, C.; Massiot, D.; Sanchez, C. Surface and bulk characterisation of titanium−oxo clusters and nanosized titania particles through ^{17}O solid state NMR. *J. Mater. Chem.* **1999**, *9*, 2467−2474.
(41) Blanchard, J.; Bonhomme, C.; Maquet, J.; Sanchez, C. Characterisation of sol−gel derived titanium oxopolymers: first evidence of Ti−OH groups through ^1H−^{17}O CP NMR experiments. *J. Mater. Chem.* **1998**, *8*, 985−989.
(42) Shi, Y.; Sun, H.; Saidi, W. A.; Nguyen, M. C.; Wang, C. Z.; Ho, K.; Yang, J.; Zhao, J. Role of Surface Stress on the Reactivity of Anatase TiO_2(001). *J. Phys. Chem. Lett.* **2017**, *8*, 1764−1771.
(43) Aschauer, U.; He, Y.; Cheng, H.; Li, S.-C.; Diebold, U.; Selloni, A. Influence of Subsurface Defects on the Surface Reactivity of TiO_2: Water on Anatase (101). *J. Phys. Chem. C* **2010**, *114*, 1278−1284.
(44) Tielens, F.; Gervais, C.; Deroy, G.; Jaber, M.; Stievano, L.; Coelho Diogo, C.; Lambert, J.-F. Characterization of Phosphate Species on Hydrated Anatase TiO_2 Surfaces. *Langmuir* **2016**, *32*, 997−1008.
(45) Walter, T. H.; Turner, G. L.; Oldfield, E. Oxygen-17 cross-polarization nmr spectroscopy of inorganic solids. *J. Magn. Reson.* **1988**, *76*, 106−120.
(46) Gervais, C.; Babonneau, F.; Smith, M. E. Detection, Quantification, and Magnetic Field Dependence of Solid-State ^{17}O NMR of X−O−Y (X,Y = Si,Ti) Linkages: Implications for Characterizing Amorphous Titania-Silica−Based Materials. *J. Phys. Chem. B* **2001**, *105*, 1971−1977.
(47) Gervais, C.; Babonneau, F.; Hoebbel, D.; Smith, M. E. Solid State NMR Interaction Parameters of Oxygens Linking Titanium and Silicon in Crystalline Cyclic Titanodiphenylsiloxanes. *Solid State Nucl. Magn. Reson.* **2000**, *17*, 2−14.
(48) Frank, O.; Zukalova, M.; Laskova, B.; Kürti, J.; Koltai, J.; Kavan, L. Raman spectra of titanium dioxide (anatase, rutile) with identified oxygen isotopes (16, 17, 18). *Phys. Chem. Chem. Phys.* **2012**, *14*, 14567−14572.
(49) Brezová, V.; Barbieriková, Z.; Zukalová, M.; Dvoranová, D.; Kavan, L. EPR study of ^{17}O-enriched titania nanopowders under UV irradiation. *Catal. Today* **2014**, *230*, 112−118.
(50) Clark, T. M.; Grandinetti, P. J.; Florian, P.; Stebbins, J. F. An ^{17}O NMR Investigation of Crystalline Sodium Metasilicate: Implications for the Determination of Local Structure in Alkali Silicates. *J. Phys. Chem. B* **2001**, *105*, 12257−12265.
(51) Larsen, F. H.; Rossano, S.; Farnan, I. Order and Disorder in Titanosilicate Glass by ^{17}O MAS, off-MAS, and 3Q-QCPMG-MAS Solid-State NMR. *J. Phys. Chem. B* **2007**, *111*, 8014−8019.
(52) Yang, S.; Park, K. D.; Oldfield, E. Oxygen-17 labeling of oxides and zeolites. *J. Am. Chem. Soc.* **1989**, *111*, 7278−7279.
(53) Boldyreva, E. Mechanochemistry of inorganic and organic systems: what is similar, what is different? *Chem. Soc. Rev.* **2013**, *42*, 7719−7738.
(54) Hutchings, B. P.; Crawford, D. E.; Gao, L.; Hu, P.; James, S. L. Feedback Kinetics in Mechanochemistry: The Importance of Cohesive States. *Angew. Chem., Int. Ed.* **2017**, *56*, 15252−15256.
(55) Kulla, H.; Haferkamp, S.; Akhmetova, I.; Röllig, M.; Maierhofer, C.; Rademann, K.; Emmerling, F. In Situ Investigations of Mechanochemical One-Pot Syntheses. *Angew. Chem., Int. Ed.* **2018**, *57*, 5930−5933.
(56) Xu, Y.; Champion, L.; Gabidullin, B.; Bryce, D. L. A kinetic study of mechanochemical halogen bond formation by in situ ^{31}P solid-state NMR spectroscopy. *Chem. Commun.* **2017**, *53*, 9930−9933.
(57) Michalchuk, A. A. L.; Tumanov, I. A.; Konar, S.; Kimber, S. A. J.; Pulham, C. R.; Boldyreva, E. V. Challenges of Mechanochemistry: Is In Situ Real-Time Quantitative Phase Analysis Always Reliable? A Case Study of Organic Salt Formation. *Advanced Sci.* **2017**, *4*, 1700132.
(58) Užarević, K.; Halasz, I.; Friščić, T. Real-Time and In Situ Monitoring of Mechanochemical Reactions: A New Playground for All Chemists. *J. Phys. Chem. Lett.* **2015**, *6*, 4129−4140.
(59) Michalchuk, A. A. L.; Tumanov, I. A.; Boldyreva, E. V. Ball size or ball mass − what matters in organic mechanochemical synthesis? *CrystEngComm* **2019**, *21*, 2174−2179.
(60) Belenguer, A. M.; Michalchuk, A. A. L.; Lampronti, G. I.; Sanders, J. K. M. Understanding the unexpected effect of frequency on the kinetics of a covalent reaction under ball-milling conditions. *Beilstein J. Org. Chem.* **2019**, *15*, 1226−1235.
(61) Gotor, F. J.; Achimovicova, M.; Real, C.; Balaz, P. Influence of the milling parameters on the mechanical work intensity in planetary mills. *Powder Technol.* **2013**, *233*, 1−7.
(62) Kulla, H.; Fischer, F.; Benemann, S.; Rademann, K.; Emmerling, F. The effect of the ball to reactant ratio on mechanochemical reaction times studied by in situ PXRD. *CrystEngComm* **2017**, *19*, 3902−3907.

https://dx.doi.org/10.1021/acs.inorgchem.0c00208
Inorg. Chem. 2020, 59, 13050−13066

(63) Zagdoun, A.; Casano, G.; Ouari, O.; Schwarzwälder, M.; Rossini, A. J.; Aussenac, F.; Yulikov, M.; Jeschke, G.; Copéret, C.; Lesage, A.; Tordo, P.; Emsley, L. Large Molecular Weight Nitroxide Biradicals Providing Efficient Dynamic Nuclear Polarization at Temperatures up to 200 K. *J. Am. Chem. Soc.* **2013**, *135*, 12790−12797.

(64) Gan, Z.; Hung, I.; Wang, X.; Paulino, J.; Wu, G.; Litvak, I. M.; Gor'kov, P. L.; Brey, W. W.; Lendi, P.; Schiano, J. L.; Bird, M. D.; Dixon, I. R.; Toth, J.; Boebinger, G. S.; Cross, T. A. NMR spectroscopy up to 35.2T using a series-connected hybrid magnet. *J. Magn. Reson.* **2017**, *284*, 125−136.

(65) Perras, F. A.; Viger-Gravel, J.; Burgess, K. M. N.; Bryce, D. L. Signal enhancement in solid-state NMR of quadrupolar nuclei. *Solid State Nucl. Magn. Reson.* **2013**, *51*−*52*, 1−15.

(66) Brinkmann, A.; Kentgens, A. P. M. Proton-Selective $^{17}O-^{1}H$ Distance Measurements in Fast Magic-Angle-Spinning Solid-State NMR Spectroscopy for the Determination of Hydrogen Bond Lengths. *J. Am. Chem. Soc.* **2006**, *128*, 14758−14759.

https://dx.doi.org/10.1021/acs.inorgchem.0c00208
Inorg. Chem. 2020, 59, 13050−13066